Moonlighting α-PheRS connects JAK/STAT with Notch signaling for intestinal homeostasis

Manh Tin Ho[1], Jiongming Lu[2], Beat Suter[1]

Affiliations:

[1]Institute of Cell Biology, University of Bern, Baltzerstrasse 4, Bern 3012, Switzerland.

[2]Present address: Max Planck Institute for Biology of Ageing, 50931 Köln, Germany.

Corresponding author: beat.suter@izb.unibe.ch

Running title: Proliferation and homeostasis function of α-PheRS

Keywords: aminoacyl tRNA synthetase, Notch signaling, JAK/STAT signaling, stem cell, differentiation, proliferation, intestinal tumor, Drosophila

Abstract

Phenylalanyl tRNA synthetase (PheRS) levels are elevated in multiple cancers and, interestingly, also in normal stem cells. Our results show that elevated levels of the *α-PheRS* subunit stimulate cell proliferation in different tissues, while downregulation of *α-PheRS* reduces organ size. Furthermore, overexpression of *α-PheRS* in stem- and progenitor cells caused over-proliferation in the intestine, a phenotype indistinguishable from the *Notch* RNAi phenotype in the same cells. Importantly, the phenotype caused by high levels of *α*-PheRS can be rescued by simultaneously overexpressing Notch, suggesting that *α-PheRS* induces this phenotype by downregulating *Notch*. High levels of α-PheRS in neuroblasts also cause the same phenotype as knocking down *Notch* in these cells, even though Notch signaling in the neuroblast lineage serves an opposite function by promoting neuroblast proliferation and maintenance. α-PheRS might, therefore, act as a general novel regulator of Notch signaling. α-PheRS levels, in turn, are controlled by Stat92E, the transcription factor of the JAK/STAT signaling pathway that is needed for the differentiation of intestinal stem cells during normal tissue homeostasis. From this, we conclude that the α-PheRS subunit can transmit the activity status of the JAK/STAT pathway to the Notch pathway as a mechanism to coordinate stem cell proliferation with differentiation. In this process, α-PheRS levels balance between tissue development and tissue growth to regulate tissue homeostasis. For its established essential function as an aminoacyl tRNA synthetase, α-PheRS needs to bind to β-PheRS in every cell to form the $\alpha_2\beta_2$ heterotetramer that loads the amino acid phenylalanine onto the cognate $tRNA^{Phe}$. Here we also demonstrate that the newly identified activities of α-PheRS are moonlighting functions, independent of the aminoacylation activity of PheRS, and they do not visibly stimulate translation.

52 # Introduction

53 Many cancer tissues display higher levels of Phenylalanyl-tRNA synthetase (PheRS, FARS or
54 FRS) than their healthy counterparts according to the database "Gene Expression across
55 Normal and Tumor tissue" (GENT2; published 11 July 2019). Interestingly, a correlation
56 between tumorigenic events and PheRS expression levels had been noted already much earlier
57 for the development of myeloid leukemia (Sen et al., 1997). Despite this, a possible causative
58 connection between elevated PheRS levels and tumor formation had so far not been reported
59 and, to our knowledge, also not been studied. This might have been due to the assumption that
60 higher PheRS levels could simply reflect the demand of tumorigenic cells for higher levels of
61 translation, or it could have to do with the difficulty of studying the moonlighting function of
62 a protein that is essential in every cell for basic cellular functions such as translation.

63 Aminoacyl-tRNA synthetases (aaRSs) are important enzymes that act by charging
64 transfer RNAs (tRNAs) with their cognate amino acid, a key process for protein translation.
65 This activity makes them essential for accurately translating the genetic information into a
66 polypeptide chain (Schimmel and Soll, 1979). Besides their well-known role in translation, an
67 increasing number of aaRSs have been found to perform additional functions in the cytoplasm,
68 the nucleus and even outside of the cell (Guo and Schimmel, 2013; Nathanson and Deutscher,
69 2000; Smirnova et al., 2012) (Casas-Tinto et al., 2015; Gomard-Mennesson et al., 2007;
70 Greenberg et al., 2008; Otani et al., 2002; Zhou et al., 2014). Moonlighting aaRSs regulate
71 alternative splicing, RNA processing and angiogenesis (Lee et al., 2004). For example, the
72 amino-acid binding site of LysRS has an immune response activity; or TrpRS inhibits the
73 vascular endothelial (VE)-cadherin, which elicits an anti-angiogenesis activity (Tzima et al.,
74 2005; Yannay-Cohen et al., 2009).

75 Cytoplasmic PheRS is one of the most complex members of the aaRSs family, a
76 heterotetrameric protein consisting of 2 alpha- (α) and 2 beta (β)-subunits responsible for
77 charging $tRNA^{Phe}$ during translation (Roy and Ibba, 2006). The α subunit includes the catalytic
78 core of the tRNA synthetase and the β subunit has structural modules with a wide range of
79 functions, including tRNA anticodon binding, hydrolyzing mis-activated amino acids, and
80 editing misaminoacylated $tRNA^{Phe}$ species (Ling et al., 2007; Lu et al., 2014; Roy and Ibba,
81 2006). Precision of the initial charging reaction and proper editing are both important for the
82 cell and the organism because mutations in the amino-acid recognition and editing sites of
83 Drosophila *PheRS* cause sieving defects that lead to mis-incorporation of amino acids into
84 proteins, ER stress, apoptosis, shortened life span, as well as neural degeneration (Lu et al.,
85 2014).

86 We set out to address the question whether and how elevated levels of PheRS can
87 contribute to tumor formation. To test for this activity, we studied the role of PheRS levels in
88 the Drosophila model system with the goal of dissecting the molecular mechanism of such a
89 moonlighting role of *PheRS.* We found that α-PheRS levels regulate cell proliferation, cell
90 differentiation or both in different tissues and cell types. We now show that elevated levels of
91 α-PheRS do not simply act to allow higher levels of translation, but control signaling
92 mechanisms involved in differentiation and proliferation control. Although the consequences
93 of altered levels vary to some degree between tissues, we found that even in two tissues with
94 the most divergent consequences, PheRS levels acted by repressing the Notch signaling
95 pathway, suggesting that this regulative mechanism is responsible for all moonlighting
96 activities of α-PheRS described here. α-PheRS levels, in turn, are controlled by JAK/STAT
97 signaling in the intestinal system, placing α-PheRS at the intersection between two signaling
98 pathways for the fine tuning of normal tissue homeostasis in the midgut. Focusing on the
99 intestine and intestinal stem cells revealed that elevated α-PheRS levels are tumorigenic in the

intestinal model. Given the high demand for research on intestinal diseases and cancer (Markowitz and Bertagnolli, 2009) our work now opens new avenues to test ways to control tissue homeostasis and tumor formation.

104 # Results

105

106 **A non-canonical α-PheRS activity is sufficient to induce additional M-phase cells**

107 To test whether elevated levels of PheRS can stimulate growth or proliferation when other
108 aaRSs are not overexpressed, we overexpressed α-PheRS, β-PheRS, and both subunits together
109 in the posterior compartment (P) of wing discs using the *engrailed-Gal4* (*en-Gal4*) driver. In
110 this assay the anterior compartment expresses normal endogenous levels and serves as an
111 internal control. When α-PheRS was overexpressed in the posterior compartment either alone
112 or together with β-PheRS, the mitotic marker phospho-histone H3 (PH3) revealed a 40%
113 increase in mitotic cells in the posterior (P) compartment relative to the anterior (A) one of the
114 same disc (Fig 1A-C). Because elevated levels of the α-PheRS subunit alone are sufficient for
115 the increase in mitotic cells, this effect is unlikely caused by increased $tRNA^{Phe}$ aminoacylation
116 activity and translational activity, which requires both subunits.

117 To test this interpretation, we made a mutant version of α-PheRS in which Tyr412 and
118 Phe438 are replaced by Cysteins. These substitutions are predicted to block the entrance into
119 the phenylalanine binding pocket, preventing binding of Phe and aminoacylation of $tRNA^{Phe}$
120 by the mutant $PheRS^{Cys}$ (Finarov et al., 2010). To test whether the $PheRS^{Cys}$ substitution indeed
121 reduces the aminoacylation activity of PheRS, we expressed mutant and wild-type α-PheRS
122 subunits together with β-PheRS subunits in E. coli, purified them and performed
123 aminoacylation assays. As opposed to the strong enzymatic activity of the wild-type α-PheRS
124 plus β-PheRS subunits, the $\alpha\text{-}PheRS^{Cys}$ together with wild-type β-PheRS produced only the
125 same background signal as the α-PheRS subunit alone (Supplementary Fig S1). The same
126 mutations were also introduced into a genomic clone and the resulting transgenic $\alpha\text{-}PheRS^{Cys}$
127 was not able to rescue the $\alpha\text{-}PheRS^{G2060}$ mutant, indicating that the Cys mutant is indeed not

128 functional in aminoacylation in vivo in Drosophila. Overexpressing a transgenic *α-PheRS*^{Cys}
129 in the posterior compartment of the wing disc also caused a 67% increase in the number of
130 mitotic cells in the above assay (Fig 1C). The fact the mutant *α-PheRS*^{Cys} version caused an
131 increase in mitotic cells at least as strongly as the wild-type *α-PheRS,* together with the fact
132 that β-PheRS overexpression was not needed for this effect, clearly demonstrates that the
133 canonical function of *PheRS* is not required to cause the elevated frequency of mitotic cells.

134 We also tested directly whether PheRS overexpression is unable to cause elevated
135 translation as we expected. For this, we analyzed general protein synthesis activity in the two
136 wing compartments by puromycin staining using the ribopuromycylation method (RPM)
137 (Deliu et al., 2017). Overexpression of the transcription factor dMyc increases protein synthesis
138 activity and was therefore used as a positive control for detection of elevated translation and
139 PMY labeling (Deliu et al., 2017). Indeed, when comparing signal intensity in the posterior
140 compartment to the intensity in the anterior compartment of the same disc, dMyc
141 overexpression significantly increased the anti-PMY signal in the expressing posterior
142 compartment. In contrast, neither overexpression of α-PheRS alone nor combined with β-
143 PheRS increased the puromycin labeling in the overexpressing compartment (Fig 1D-E'', F).
144 The combined results therefore demonstrate unambiguously that elevated α-PheRS levels
145 cause additional cells to be in mitosis through an aminoacylation- and translation-independent,
146 non-canonical activity. α-PheRS levels might specifically slow down progression through M-
147 phase, causing higher numbers of cells to remain in the PH3-positive state. Alternatively, they
148 might either promote over-proliferation of mitotic cells or induce proliferation in non-cycling
149 cells.

150

151 **High α-PheRS tolerance in an organ with tight size control**

152 To find out whether the increased number of mitotic cells in the region expressing higher α-
153 PheRS levels leads to a different compartment size, we measured the size of two clearly defined
154 regions in the posterior (P) and the anterior (A) compartment of the adult wing as shown in Fig
155 2A. Normalizing the size of the posterior region (P) to the size of the anterior region (A), we
156 calculated the P/A ratio (Fig 2B). Even though α-PheRS alone was sufficient to induce
157 additional mitotic cells in larval discs, this did not cause the formation of a larger wing in the
158 adult. Co-overexpression of both subunits was needed to cause a small, but significant increase
159 of the posterior region of the wing (Fig 2B). This size increase does not appear to be a general
160 property of elevated aaRS levels because overexpression of Glycyl-tRNA synthetase (GlyRS;
161 (Niehues et al., 2015)) with the same driver did not increase wing size (Fig 2B). The final size
162 of this particular organ is tightly controlled by different mechanisms that are only partially
163 understood, but are capable of compensating for differences in growth and proliferation such
164 that the compartments reach their correct final size even if they grew at different rates at an
165 earlier stage (Hariharan, 2015; Martin and Morata, 2006). To better understand the
166 consequences of high PheRS levels in the discs, we studied its effect on dissociated cells and
167 found that elevated PheRS levels primarily affected cell size, whereas proliferation remained
168 controlled or was compensated for (Supplementary data, Fig S2A,B).

169 We considered the possibility that PheRS might signal availability of Phe to TORC1,
170 which links cell growth to amino acid availability (Laplante and Sabatini, 2012; Wullschleger
171 et al., 2006). Such a mechanism would be analogous to the function of LeuRS in this pathway
172 (Bonfils et al., 2012; Han et al., 2012). However, experimental testing of this hypothesis did
173 not uncover any evidence for such a signaling function (Supplementary data, Fig S3A,B).

174

175 **The *α-PheRS* subunit accelerates proliferation in different tissues and its knockdown**
176 **reduces organ size**

177 To test the effects of PheRS levels on proliferation directly and in a different organ and cell
178 type, we set up a mosaic analysis with repressible cell marker (MARCM; (Wu and Luo, 2006)
179 assay in the follicle cells. Twin spot clones were generated with one clone overexpressing
180 PheRS and the GFP marker, and its twin clone expressing normal endogenous levels of PheRS
181 and serving as an internal control (Fig 3A). The results of this experiment showed that clonal
182 overexpression of both subunits of PheRS accelerated the proliferation of the overexpressing
183 cells on average by 32% (Fig 3B). Overexpression of GFP with only the β-PheRS subunit or
184 with GlyRS did not significantly promote clonal expansion (Fig 3B), confirming that the
185 activity of stimulating growth and proliferation is specific for PheRS and not a general role of
186 aaRSs. Interestingly, overexpression of GFP with the α-PheRS subunit alone also stimulated
187 cell proliferation autonomously by 30% (Fig 3B) and, intriguingly, this was very close to the
188 32% increase calculated for the clone overexpressing both PheRS subunits (Fig 3B).
189 Remarkably, the higher number of mitotic cells observed upon α-PheRS overexpression in the
190 posterior compartment of the larval wing discs (Fig 1C) was in a comparable range as the
191 proliferation increase in the follicle cell assay (Fig 3B). These results therefore show that α-
192 PheRS levels promote cell proliferation and they suggest that it has this activity in different
193 tissues.

194 Overexpression of *α-PheRS*^{Cys} alone and *α-PheRS*^{Cys} together with *β-PheRS (PheRS*^{Cys}) 195 stimulated clonal growth and cell proliferation in the follicle cell twin spot experiment by 28%
196 and 25%, respectively (Fig 3B), again confirming that this is an aminoacylation-independent
197 activity. It is tempting to speculate that the slightly lower increase in proliferation upon

198 overexpressing the mutant *α-PheRS*^{Cys} (28%) in twin spot clones compared to wild-type *α-*
199 *PheRS* (30%) could be due to reduced translation caused by the overexpression of an inactive
200 α subunit that is predicted to partially act as a dominant negative subunit for the aminoacylation
201 function. If this proliferation function is important for development and homeostasis, reduced
202 *α-PheRS* activity should lead to problems in these processes. Because *α-PheRS* and *β-PheRS*
203 are both essential genes in Drosophila (Lu et al., 2014), we used RNAi to reduce their activity
204 in specific tissues by RNAi (Fig S4A,B). Indeed, knock down in the developing eye reduced
205 the adult eye, whereas knockdown in the larval fat body reduced the size of the entire pupae.
206 Furthermore, RNAi knockdown *α-PheRS* or *β-PheRS* in Kc cells caused these cells to
207 proliferate more slowly than the control cells (Fig S4C). Although it is not clear from these
208 results, which activity of PheRS causes this effect, the phenotypes observed are consistent with
209 a direct function in regulating proliferation.

210

211 **α-PheRS promotes stem cell proliferation in the midgut and high expression leads to**
212 **hyper- and dysplasia**

213 Tissue growth and homeostasis play important roles in developing and outgrown animals, and
214 they require tight control of stem cell self-renewal and differentiation of daughter cells. The
215 Drosophila midgut is a powerful model to analyze these mechanisms and their interplay.
216 Intestinal stem cells (ISCs), also referred to as adult midgut progenitors (AMPs) in the larval
217 gut, can either divide asymmetrically or symmetrically. After an asymmetric division, one
218 daughter cell differentiates into an absorptive enterocyte (EC) or a secretory enteroendocrine
219 (EE) cell, the other keeps its stem cell identity (Micchelli and Perrimon, 2006; Ohlstein and
220 Spradling, 2007). We investigated the effect of overexpression of each PheRS subunit in larval
221 ISCs by using the *esg-Gal4* driver, which expresses specifically in ISCs. Co-expression of

222 *UAS-YFP* allowed us to monitor the *esg-Gal4* activity. The results demonstrated that
223 overexpression of Myc::α-PheRS alone in the larval midgut caused the numbers of YFP
224 positive ISC cell clusters in the posterior midgut to increase. In addition, the number of YFP
225 positive cells per cluster increased as well (Fig 4A, B, D-D'). The increase of both numbers
226 was significant when compared to posterior midguts expressing normal levels of α-PheRS (Fig
227 4A, B, C-C'). Overexpression of β-PheRS::V5 alone did not produce such a phenotype (Fig
228 4A, B, E-E'). Interestingly, when both PheRS subunits were overexpressed, the guts also
229 showed an increase in the number of YFP positive ISC clusters. However, the increase was
230 less pronounced and the number of YFP positive cells per cluster remained unchanged (Fig
231 4A, B, F-F').

232 Driving the expression of the α-PheRS^{Cys} mutant alone in ISCs also produced
233 additional ISCs, indicating again that the aminoacylation function is not required for this
234 activity (Fig 4G). Surprisingly, however, this treatment induced the over-proliferative
235 phenotype in both anterior and posterior areas of the larval midgut (outlined with white dashed
236 lines, Fig 4G, G') while the overexpression of wild-type Myc::α-PheRS gave rise to high
237 numbers of ISCs only in the posterior midgut (Fig 4D, D'). Interestingly, elevated α-PheRS^{Cys}
238 levels also caused the appearance of a more severe, tumor-like phenotype, where individual
239 ISC clusters could not be discerned anymore. Furthermore, instead of the wild-type gut
240 phenotype, characterized by a majority of ECs with large nuclei, interspersed with occasional
241 ISC clusters with smaller nuclei (as seen in the YFP overexpression control, Fig 4C, C'), we
242 observed a phenotype where ECs and ISCs could not be distinguished based on the size of their
243 nuclei, but emerged as a larger cell population with intermediate size nuclei (Fig 4G'). Many
244 of these cells expressed the *esg*>YFP stem cell marker at high levels, but others displayed only
245 a very weak YFP signal. One possible interpretation of this phenotype could be that α-PheRS^{Cys}
246 overexpressing ISCs progress through the cell cycle more rapidly such that they are not able to

247 grow to their proper size and do not have sufficient time to turn over the YFP. Staining these
248 guts for the mitotic marker PH3 demonstrated that the posterior midgut contained clearly more
249 and a higher proportion of PH3 positive cells. Significantly, more cells were labelled by anti
250 PH3 staining in the posterior midgut when α-PheRS or the α-PheRS^{Cys} mutant were
251 overexpressed alone in ISCs (Fig 4H, I). Again, this suggests that cells in these areas display
252 an elevated proliferation rate.

253 In a normal adult midgut, ISCs are found as characteristic single cells or as pairs with
254 their daughter enteroblast (EB). Both cell types are labeled with YFP when their expression is
255 driven by *esg*-Gal4 (Fig 4J). Overexpression of only α-PheRS or α-PheRS^{Cys} in these adult
256 ISCs caused a strong phenotype, too. It induced hyperplasia and dysplasia in regions R4-R5 of
257 the posterior midgut. Similar to the hyperplasia phenotype observed in the larval gut, we
258 observed cells adjacent to ISC clusters displaying the YFP stem cell marker, even though they
259 contained large nuclei (Fig 4J'-J"), indicative of a dysplasia phenotype. We conclude that in
260 the larval and adult guts, elevated α-PheRS expression can elevate the proliferation rate of stem
261 cells and lead to hyper- and dysplasia.

262

263 **Elevated α-PheRS levels prevent proper differentiation and gut homeostasis by**
264 **downregulating Notch signaling**

265 Asymmetric divisions of ISCs give rise to a new ISC and an undifferentiated EB. Differential
266 Delta/Notch signaling between the new ISC and the EB causes the latter to either differentiate
267 into an absorptive EC or a secretory EE (Micchelli and Perrimon, 2006; Ohlstein and Spradling,
268 2007). To investigate how α-PheRS affects the fate decision in this lineage, we studied the cell
269 population in the posterior midgut. In larval and adult guts, the over-proliferation phenotype
270 caused by α-PheRS^{Cys} overexpression showed a significantly elevated ratio between EEs and

271 ECs (Fig 5A-A', B-B', C). The overexpression of *α-PheRS* alone with the *esg-Gal4* driver
272 caused the same changes, albeit with a slightly lower expressivity (Fig 5C). These observations
273 indicate that overexpression of α-PheRS or α-PheRS^{Cys} directs EB differentiation to the EE
274 fate and interferes with EC differentiation.

275 Differentiating ISC daughter cells, EBs, adopt the EE fate when their *Notch* activity is
276 low and the EC fate if their *Notch* activity is high (Takashima et al., 2011). Furthermore,
277 because *Notch* activity is needed for EB differentiation, reduced *Notch* activity leads to EE-
278 like and ISC-like tumors (Micchelli and Perrimon, 2006; Patel et al., 2015; Wang et al., 2015;
279 Yin and Xi, 2018). Indeed, in regions where the normal cellular composition of the larval gut
280 was transformed, we observed an increase in the number of cells and in particular a cell
281 population with intermediate size nuclei upon RNAi treatment of *Notch* with the *esg-Gal4*
282 driver (white dashed line, Fig 5D-D'). The similarity between the two phenotypes suggests that
283 overexpression of *α-PheRS* or *α-PheRS^{Cys}* might cause this phenotype by reducing *Notch*
284 activity. Indeed, as seen in Fig 5F, overexpression of *α-PheRS* and *α-PheRS^{Cys}* downregulates
285 the *Notch* activity reporter NRE-EGFP (Notch response element promoter driving the
286 expression of eGFP; (Housden et al., 2012) and overexpressing *Notch* together with *α-*
287 *PheRS^{Cys}* in the same midgut ISCs rescued the tumor-like midgut phenotype, giving rise to
288 midguts with a wild-type appearance (Fig 5A", B", E-E'). This shows that α-PheRS levels
289 control *Notch* activity and that high α-PheRS levels cause the tumor-like phenotype in the
290 midgut by downregulating *Notch* activity.

291

292 **_α-PheRS_ is a novel general repressor of Notch signaling**

293 Developing larval brains contain neuroblast (NB) stem cells that divide asymmetrically to
294 either keep the stemness and or to differentiate into neuronal cells. *Notch* signaling plays a

295 crucial role in this process (Ables et al., 2011; Giachino and Taylor, 2014), but in contrast to
296 the situation in the gut, loss of *Notch* prevents NB self-renewal, and ectopic expression of *Notch*
297 leads to tumor formation (de la Pompa et al., 1997; Grandbarbe et al., 2003; Hatakeyama et al.,
298 2004). This opposite role of *Notch* makes the NB lineage an ideal complementary system to
299 test whether α-PheRS is a general component of the *Notch* pathway. Driving α-PheRS or the
300 α-PheRS^{Cys} expression in NBs with the *inscutable-Gal4 (incs-Gal4)* driver resulted in
301 significantly smaller central brains (CB), the region where the NBs are located (Fig 6A-A'',
302 B). In contrast, this treatment had little or no effect on the size of the optic lobes (OL). The
303 phenotype was indistinguishable from the phenotype caused by *Notch* knock-down (Fig 6B),
304 and co-overexpression of Notch with α-PheRS^{Cys} in neuroblasts rescued the brains to wild-
305 type size (Fig 6B).

306 Type II neuroblasts are particularly suited to analyze effects on neuroblast
307 differentiation. Targeting specifically the 8 type II neuroblasts in central brain lobes with *α-*
308 *PheRS* or *α-PheRS*^{Cys,} overexpression, resulted in half of the central brains in a strong reduction
309 of the number of neuroblasts, and the resulting central brain lobes ended up smaller (Fig 6C
310 and Supplementary Fig S5). Knocking down *Notch* in type II NBs with RNAi and the same
311 driver combination resulted in a similar phenotype, but with a higher expressivity. On the other
312 hand, overexpression of Notch in α-PheRS overexpressing type II neuroblasts partially rescued
313 the number of type II neuroblasts to wild-type numbers and it restored the normal size of the
314 brain (Fig 6C and Supplementary Fig S5). Because the effect on Notch signaling is the same
315 in guts and brains, two tissues where *Notch* has opposing functions on cellular differentiation,
316 we conclude that *α-PheRS* is a novel general repressor of Notch signaling.

317

318 **Transcription factor Stat92E of the JAK/STAT pathway regulates α-PheRS levels**

319 Under normal conditions, the JAK/STAT signaling pathway induces progenitor differentiation
320 into ECs via regulating Notch activity (Herrera and Bach, 2019). Under stress conditions like
321 bacterial infection, secreted Unpaired3 (Upd3) acts as a cytokine that activates JAK/STAT
322 signaling, leading to ISC proliferation and differentiation to repair the damaged parts of the gut
323 (Buchon et al., 2009; Lin et al., 2010). Upd3 not only activates JAK/STAT signaling, but also
324 *Notch* activity to enhance ISC proliferation and to promote EC differentiation, respectively
325 (Jiang et al., 2009). Because α-PheRS levels affect Notch signaling, too, we therefore tested
326 whether α-PheRS could possibly coordinate JAK/STAT with Notch signaling. The *Stat92E*
327 gene encodes the transcription factor at the downstream end of the JAK/STAT pathway. Using
328 the hypomorphic $Stat92E^{HJ}$ allele, we tested whether suppressing JAK/STAT signaling affects
329 α-PheRS expression. Indeed, $Stat92E^{HJ}$ mutants displayed elevated levels of α-PheRS in Delta-
330 positive ISC cells (Fig 7A-B"). Consistent with this result, *Stat92E* knock-down by RNAi with
331 the *esg-Gal4* driver also showed elevated α-PheRS levels in ISC cells (Fig7C-C"). As shown
332 in Fig 7 D-D', E-E', F-F', G, the levels of α-PheRS significantly increased in ISCs/EBs. The
333 fact that two different approaches to reduce *Stat92E* activity lead to higher α-PheRS levels in
334 ISCs/EBs clearly demonstrates that *Stat92E* regulates α-PheRS levels in these cells.

335 Surprisingly, RNAi knock down of *Stat92E* with the *esg-Gal4* driver not only affected
336 α-PheRS levels in ISCs, but also in some neighboring polyploid ECs, but not in distant ECs
337 (arrows in Fig7C", F) (Fig7G). Because we also observed this phenotype in $Stat92E^{HJ}$ mutants
338 (arrows in Fig 7E) (Fig 7G), this is unlikely to be an off-target effect of the RNAi. It thus
339 appears that *Stat92E* can normally control α-PheRS levels also in a cell non-autonomous way.
340 To test if *Stat92E* is not only required for downregulation of α-PheRS, but also sufficient, we
341 overexpressed *Stat92E* in ISCs and EBs. Indeed, elevated-Stat92E levels reduced the α-PheRS
342 signal in ISCs and EBs (Fig 7H-I"). On the other hand, high levels of α-PheRS did not affect

343 *Stat92E* activity when assayed with the *10X STAT92E-GFP* reporter (Bach et al., 2007) (Fig
344 7J-K'''). We conclude that *Stat92E* can regulate α-PheRS levels specifically in EBs and ISCs
345 to maintain stem cell homeostasis. Together with the result that α-PheRS regulates Notch
346 signaling, we therefore identified α-PheRS as an intermediate factor that links the JAK/STAT
347 pathway to Notch signaling to regulate gut homeostasis.

348

349 # Discussion

350 Our work revealed that *PheRS* not only charges tRNAs with their cognate amino acid Phe, but
351 that it also performs moonlighting functions in regulating cell proliferation and differentiation
352 in different tissues. Levels of α-PheRS are critical for these regulative processes and these
353 levels are generally elevated in healthy stem cells compared to differentiated cells. Similarly,
354 many tumor cells show elevated α-PheRS levels compared to their healthy counterparts and a
355 positive correlation between these levels and tumorigenic events had been noted quite some
356 time ago (Sen et al., 1997). Several circumstantial and direct evidence show that elevated α-
357 PheRS levels do not simply allow higher translational activity to overcome a growth rate
358 restriction imposed by hypothetically limiting levels of PheRS. In fact, PheRS is unlikely to be
359 rate-limiting for cellular growth. because animals with only one copy of the *α-PheRS* or *β-*
360 *PheRS* gene do not show a phenotype (Lu et al., 2014) and tissue culture cells can be stimulated
361 to grow more rapidly without stimulating the expression of the two PheRS genes (Chen et al.,
362 2003) (Lu et al., 2014). Indeed, directly measuring translational activity *in situ* (Fig 1D-D")
363 showed the same levels of translation whether *α-PheRS* was overexpressed or not.
364 Furthermore, aminoacylation of $tRNA^{Phe}$ requires the tetrameric protein $\alpha_2\beta_2$*-PheRS.* However,
365 overexpression of an aminoacylation-dead α*-PheRS*^{Cys} mutant subunit alone, (without
366 simultaneous overexpression of the β-PheRS subunit) already lead to the accumulation of
367 numerous additional dividing cells, closely resembling the phenotype observed when the wild-
368 type gene was expressed in the same way. We therefore conclude that this activity of *α-PheRS*
369 is independent of the translational function of *PheRS*.

370 The notion that the α-PheRS subunit can be stable and it functions independently of the
371 β-subunit was surprising because previous results showed that the two subunits were dependent
372 on the presence of the other subunit for their stability (Antonellis et al., 2018; Lu et al., 2014).

373 Our results now show that this requirement does not apply to all cell types. In young follicle
374 cells, ISCs and possibly other dividing cells, the overexpression of the α-PheRS subunit alone
375 results in higher levels of α-PheRS accumulation and, in particular when elevated levels were
376 induced in gut ISCs and EBs, this produced a strong phenotype. This suggests that the α- and
377 β-PheRS subunits function together in every cell to aminoacylate $tRNA^{Phe}$, but in addition, the
378 α-subunit can be stable in specific cell types, such as stem cells, where it assumed a novel
379 function in regulating cell proliferation and differentiation.

380 PheRS is not the only aaRS family member for which roles beyond charging tRNAs
381 have been identified (Dolde et al., 2014). For instance, MetRS/MRS is capable of stimulating
382 the rRNA synthesis (Ko et al., 2000), GlnRS/QRS can block the kinase activity of apoptosis
383 signal-regulating kinase 1 (ASK1) (Ko et al., 2001) and a proteolytically processed form of
384 YARS/TyrRS acts as a cytokine (Casas-Tinto et al., 2015; Greenberg et al., 2008). aaRSs are,
385 however, also not the only protein family which evolved to carry out more than one function.
386 In recent years it has become increasingly evident that many if not most proteins have evolved
387 to carry out not only one, but two or more functions, providing interesting challenges to figure
388 out, which of their activities are important for the individual functions of a protein (Dolde et
389 al., 2014).

390 We found that elevated levels of α-PheRS promote cell proliferation in different cell
391 types. In follicle cells, more cells were produced in the α-PheRS overexpressing clones
392 compared to wild-type clones. In wing disc, more mitotic cells were detected in the α-PheRS
393 overexpressing compartments. In the gut tissue, elevated $\alpha\text{-PheRS}^{(Cys)}$ levels produced 2-5
394 times as many cells with intermediate size nuclei that stained positive for stem cell markers.
395 Similarly, these guts also contained 5-8 times as many mitotic cells when $\alpha\text{-PheRS}^{(Cys)}$ was
396 overexpressed. Together, these results strongly suggest, that also in this situation the higher

397 levels of α-PheRS induced over-proliferation of ISCs. These phenotypes are not only
398 independent of the aaRS activity (Fig 1D-F), they also do not reflect a function in sensing the
399 availability of its enzymatic substrate Phe and transmitting this information to the major growth
400 controller, the TOR pathway (Fig S3). The proliferation activity of α-PheRS is therefore
401 fundamentally different from the growth supporting activity of the aaRS members TrpRS or
402 LeuRS (Adam et al., 2018; Bonfils et al., 2012; Han et al., 2012).

403 Overexpression of α-PheRS in the gut ISCs additionally interfered with cell fate
404 decisions by driving ISCs to duplicate and to differentiate into EEs. The combination of these
405 effects results in a "tumor-like" phenotype, that had been described as ISC/EE tumor phenotype
406 that results from downregulation of *Notch* activity (Korzelius et al., 2014; Micchelli and
407 Perrimon, 2006). Interestingly, mis-regulating proteins involved in EE fate specification, like
408 downregulation of Tramtrack69 or upregulation of its adaptor protein Phyllopod, also results
409 in this phenotype (Wang et al., 2015; Yin and Xi, 2018), suggesting that α-PheRS levels,
410 through their activity on Notch signaling, induce the "tumor-like" phenotype in the gut tissue
411 not only by increasing stem cell proliferation, but also by driving differentiating cells into an
412 EE fate.

413 The gut phenotype caused by elevated levels of α-PheRS points to the importance of
414 controlling and fine tuning these levels. We found that the JAK/STAT pathway has the
415 capability of modulating cellular α-PheRS levels. Interestingly, JAK/STAT signaling, which
416 stimulates progenitor cell differentiation during normal tissue homeostasis (Herrera and Bach,
417 2019), downregulates *α-PheRS* levels, which consequently allows higher Notch signaling to
418 promote differentiation of the EB progenitor cells into ECs. Therefore, regulation of α-PheRS
419 levels links the two signaling pathways and implicates α-PheRS not only in promoting cell
420 proliferation, but also in regulating stem cell and tissue homeostasis by connecting the Notch

421 to the JAK/STAT signaling pathway. Stat92E is a transcription factor, but none of the
422 published reports on Stat92E targets lists the *α-PheRS* gene (Bina et al., 2010; Muller et al.,
423 2005; Wang et al., 2013). A direct repression of *α-PheRS* gene expression by Stat92E appears
424 therefore unlikely, even though it is also possible that this interaction escaped detection because
425 it happens in too few cells of the analyzed cell types.

426 An interplay between the JAK/STAT and the Notch signaling pathways to maintain
427 ISC homeostasis has been noted before in regenerating midguts. In this situation, damaged ECs
428 release Upd cytokines to activate JAK/STAT signaling in ISCs and to promote ISC division
429 (Jiang et al., 2009). This also stimulates Delta/Notch activity to promote EC differentiation
430 (Jiang et al., 2009). Knocking down *Stat92E* reduced Notch signaling, and Notch target genes
431 were downregulated when *Stat92E* activity was abolished in progenitor cells (Jiang et al.,
432 2009). JAK/STAT signaling therefore feeds into the downstream Notch signaling pathway
433 under these conditions, too. Our work revealed an unexpected missing link between the two
434 signaling pathways in normal tissue homeostasis and it would therefore be interesting to also
435 explore the function of *α-PheRS* in these pathways during tissue regeneration.

436

437 **Relevance of moonlighting function of α-PheRS for tumor formation**

438 Several aaRSs have come into the focus of cancer research (Kim et al., 2014). For instance,
439 LeuRS senses the availability of the amino acid Leu and if these levels are sufficient to support
440 growth, it signals a growth readiness to the key growth controller TORC1/mTORC1 (Bonfils
441 et al., 2012; Han et al., 2012). Our results suggest that PheRS does not serve an analogous
442 function as a Phe sensor (Suppl. Figure S3). Phe binding appears to be dispensable to activate
443 proliferation and to repress *Notch* signaling because the α-PheRS^{Cys} mutant, in which two
444 essential residues in the Phe binding pocket were replaced by Cys is unable to perform

445 aminoacylation (presumably because it cannot bind Phe), but still able to induce the non-
446 canonical activity.

447 Improper expression of PheRS was suspected long ago to promote carcinogenesis, but
448 till now the mechanisms behind this effect remind unknown. Elevated levels of *FARSA/CML33*
449 (human α-PheRS) during the development of myeloid leukemia have been demonstrated to
450 directly correlate with tumorigenic events (Sen et al., 1997). The GENT2 database published
451 in 2019 describes also strong positive correlations between PheRS subunit levels and
452 tumorigenic events in several tissues and cancers, including colon cancer, which mostly seems
453 to originate from intestinal stem cells (ISCs) (Barker et al., 2009). Modelling the effect of
454 elevated α-PheRS levels in *Drosophila* ISCs and CBs, we found that these levels lead to over-
455 proliferation of cells with stem cell characteristics and to changes in cell fate, indicating that
456 elevated α-PheRS levels can indeed be a risk factor for tumor formation.

457 Modeling the effects of elevated α-PheRS levels in ISCs revealed that
458 hyperaccumulation of stem cells, a tumor risk, is mediated by high α-PheRS repressing Notch
459 signaling. In mammals, Notch signaling is essential for maintaining the homeostasis of cell
460 proliferation and differentiation (Qiao and Wong, 2009), similar to the function of Notch
461 signaling in the Drosophila gut that is needed to prevent the induction of enteroendocrine
462 tumors characterized by excessive EEs and ISCs in the adult midgut (Micchelli and Perrimon,
463 2006; Ohlstein and Spradling, 2007). Because in human, mis-regulation of Notch signaling in
464 these processes has been suggested to trigger the development of colon cancer, *Notch* has been
465 proposed as a molecular target for cancer therapy (Yin et al., 2010). The results presented here
466 provide new and unexpected insights into the communication between two major signaling
467 pathways involved in gut tumorigenesis and they suggest new opportunities to target these
468 mechanisms.

469 # Materials and Methods

470 **Key Resources Table**

Reagent or Resource	Sources	Identifier	Additional information
Antibodies			
Anti phospho-Histone H3-rabbit	Cell signaling	9701S	1:200 v/v
Anti phospho-Histone H3-mouse	Cell signaling	9706S	1:200 v/v
Anti *α-PheRS*	Genescript	4668	Customized product (1:200 v/v)
Anti *α-PheRS*	Genescript	4669	Customized product (1:200 v/v)
Anti Myc-mouse	Developmental Studies Hybridoma Bank (DSHB)	9E10	Supernatant (1:3 v/v)
Anti Puromycin	DSHB	PMY-2A4	1:100 v/v
Anti Prospero	DSHB	MR1A	1:200 v/v
Anti Delta	DSHB	C594.9B	1:10 v/v
Anti V5 tag-rabbit	Cell signaling	13202	1:200 v/v
Anti Cy3 rabbit	Jackson Immuno Research	115-165-146	1:200 v/v
Anti-rabbit Alexa Flour 488	Molecular Probes	A-11008	1:200 v/v
Anti-rabbit Alexa Flour 488	Molecular Probes	A-11034	1:200 v/v
Anti-mouse Alexa Flour 488	Molecular Probes	A-11029	1:200 v/v
Anti-rabbit Alexa Flour 488	Life technology	A-21206	1:200 v/v
Anti-rabbit Alexa Flour 594	Invitrogen	A-11037	1:200 v/v
Anti-mouse Alexa Flour 594	Molecular Probes	A-11032	1:200 v/v
Anti-mouse Alexa Flour 568	Life technology	A-10037	1:200 v/v
Anti α-tubulin	Abcam	Ab18251	1:1,000 v/v
Anti GFP	ImmunoKontact	042704	1:1,000 v/v
Anti Myc-rabbit	Santa Cruz	Sc-789	A-12 (1:1,000 v/v)
HRP Anti rabbit IgG antibody (Peroxidase)	Vector	PI-1000	1:10,000 v/v
HRP Anti rabbit IgG antibody (Peroxidase)	Vector	PI-2000	1:10,000 v/v

471

Fly stocks and genetics			
α-PheRS^{G2060}/FM6	Bloomington Drosophila Stock Center (BDSC)	26625	
RNAi- α-PheRS	Vienna Drosophila RNAi Center (VDRC)	33514	
RNAi- β-PheRS	VDRC	42046	
eyeless-Gal4	BDSC	5535	
engrailed-Gal4	BDSC	30564	
UAS-GFP	BDSC	6658	
STAT92E[HJ]/TM3,Sb	BDSC	24510	
w; UAS-Myc::MYC	BDSC	9674	
hspFLP/y ; + ; UAS-Myc::MYC	BDSC	9675	
hspFLP/y ; UAS-N^{ICD} /CyO ; MKRS/TM2	BDSC	52008	
10X STAT92E GFP	BDSC	26197	
UAS-N RNAi	BDSC	33611	
UAS-N RNAi	BDSC	7078	
*neoFRT*82B *Sb1*/TM6	BDSC	2051	
NRE-EGFP	BDSC	30728	
UAS-Dl	BDSC	5614	
tub-Gal4/TM3,Sb	BDSC	5138	
y w att2A[vas-ϕ]; +; attP-86F	ETH Zurich		A gift from Hugo Stocker, ETH
esg-Gal4,UAS-2XEYFP;MKRS/TM6B,Tb	ETH Zurich		A gift from Hugo Stocker, ETH
yw; esg-Gal4, UAS-GFP/TM6B,Tb,Hu	ETH Zurich	2400	A gift from Hugo Stocker, ETH
NP1-Gal4 (Myo31DF)/CyO y+	ETH Zurich	2398	A gift from Hugo Stocker, ETH
esg-Gal4, UAS-mCherry-CD8, tub-gal80^{ts}/CyO			A gift from Péter Nagy, Cornell University
yw;UAS-cyto-gars-myc/CyO			A gift from Albena Jordanova, VIB-U Antwerp Center for Molecular Neurology

472

Bacteria strains and vectors		
XL1 blue	Aligent	200249
Rosseta – Novagen	Merckmilipore	70954
pET-28a – Novagen	Merckmilipore	69864
pET LIC (2A-T)	Addgene	29665
pUASattB	Drosophila Genomics Resource Center	1419
pw+SNattB	(Koch et al., 2009)	
Commercial assay or kit		
Pierce® Silver Stain kit	Thermo Scientific	24612
Pierce® BCA Protein Assay kit	Thermo Scientific	23227
ReliaPrep™ DNA CleanUp and Concentration System	Promega	A2893
GeneElute™ HP Plasmid miniprep kit	Sigma	NA0160
Qiagen® Plasmid Plus Midi kit	Qiagen	12943
Ni-NTA affinity resin	Qiagen	30210
ECL™ Prime Western Blotting System	GE Healthcare	RPN2232
RNAMaxx™ High Yield Transcription Kit	Aligent	200339
Software, algorithm		
Leica Application Suite X (LAS X)	Leica	https://www.leica-microsystems.com/products/microscope-software/p/leica-las-x-ls/
FIJI	ImageJ	https://fiji.sc/
GraphPad Prism	GraphPad	https://www.graphpad.com/scientific-software/prism/
FlowJo™	BD Biosciences	https://www.flowjo.com/
Microsoft Excel	Microsoft	https://products.office.com/en-us/excel

473

474 **Buffers**

Lysis buffer for Drosophila tissue	**Lysis buffer for bacteria**
20 mM Tris HCl pH7.4 150uM NaCl 2 mM EDTA 50 mM NaF 10% Glycerol 1% Triton X100 1 Protease inhibitor cocktail tablet (Roche-4693159001)	20 mM Tris HCl pH7.4 150uM NaCl 2 mM EDTA 50 mM NaF 10% Glycerol 1% Triton X100 4mM Imidazole 1M 0.6% Lysozyme

1 mM phenylmethylsulphonyl fluoride	1 Protease inhibitor cocktail tablet 1 mM phenylmethylsulphonyl fluoride
4% PFA	**1X PBST**
1X PBST 4% (w/v) Paraformaldehyde	0.2 % (v/v) Tween 20 1X PBS
Blocking buffer	**Fly food recipe**
5% (w/v) non-fat dry milk 0.1% (v/v) Triton X100	20.4 l H_20 1,680 g Maize flour 720 g Yeast 1,800 g Syrup 192 g Potassium sodium tartrate tetrahydrate 36 g Nipagin 120 ml Propionic acid
10X PBS pH 7.4	
10.6 mM KH_2PO_4 1.5 M NaCl 30 mM $Na_2PO_4.7H_20$	
10X SDS running buffer	**10X Transfer buffer**
30 g Tris base 144 g Glycine 10 g SDS dH_2O to 1ℓ	30 g Tris base 144 g Glycine dH_2O to 1ℓ
10X TBS pH to 7.6	**1X TBST**
24 g of Tris Base 88 g of NaCl dH_2O to 1ℓ	100 mL 10X TBS 900 mL dH_2O 0.1% (v/v) Tween 20

475

476 **Primers**

Name	Sequence (5' to 3')	Application
rc2263f	CGCGGATCCATCCGGCGAGAGAGTGTCTTTG	Genomic genomic construct of *α-PheRS*
rc2263r	CGGGGTACCTATGCCTGGCGATAATCGTG	
Tyr412Cys & Phe438Cys-F	TCAAGCCGGCGTACAATCCGTGTACCGAGCCCAG	Construct of *α-PheRS*^{Cys} mutation
Tyr412Cys & Phe438Cys-R	CTCCGGCCGACAGACGCCCGAGTTGCCC	
α-PheRS RNAi 11f	TAATACGACTCACTATAGGGAGGCAAGAAACGCAAGCTCCTC	*α-PheRS* ds RNA synthesis
α-PheRS RNAi 11r	TAATACGACTCACTATAGGGAGGGAACTCCGCCAGATGTGTG	
β-PheRS RNAi 10f	TAATACGACTCACTATAGGGAGGGCCAATCATTCGGGAATCA	*β-PheRS* ds RNA synthesis
β-PheRS RNAi 10r	TAATACGACTCACTATAGGGAGGAGGCAGGGACTTCTTAATGT	
seq r6	GCTCCCATTCATCAGTTCC	Sequencing
seqA r1	CATTTCCACCGTGAGATCCGTC	Sequencing
seqA r2	AACTCTTGTGGGTGACCGTTTC	Sequencing
seqA f1	GTTCTCGAAGTGAATGTTCTGG	Sequencing

seqA f2	TTTAGCCACCGTCGTCGTTTC	Sequencing
seqA r3	TCCAGCGACGATGACGAATTTG	Sequencing
seqA f3	CAAATGGATTGTGGGACCAGC	Sequencing
seqA r4	GCCCTCCTCCACCATCTTTAG	Sequencing

477

478 **Fly genetics and husbandry**

479 All *Drosophila melanogaster* fly stocks were kept for long term storage at 18ºC in glass or
480 plastic vials on standard food with day/night (12h/12h) light cycles. All experiments were
481 performed at 25ºC unless specifically mentioned. A UAS-GFP element was added in the
482 crosses of all rescue experiments to even out the effect of Gal4 by providing the same number
483 of UAS constructs. Origins of all stocks are noted in the *Key Resource Table*.

484

485 **DNA cloning and generation of transgenic flies**

486 Sequence information was obtained from Flybase. All mutations and the addition of the Myc-
487 tag to the N-terminus of *α-PheRS* were made by following the procedure of the QuickChange®
488 Site-Directed Mutagenesis Kit (Stratagene). The genomic *α-PheRS* rescue construct (*Myc::α-*
489 *PheRS*) codes for the entire coding region and for an additional Myc tag at the N-terminal end.
490 In addition, it contains ~ 1kb of up- and down-stream sequences and it was cloned into the
491 *pw$^+$SNattB* transformation vector (Koch et al., 2009; Lu et al., 2014). The *α-PheRS* and *β-*
492 *PheRS* cDNAs were obtained by RT-PCR from mRNA isolated from 4-8 days old *OreR* flies
493 (Lu et al., 2014). The Tyr412Cys and Phe438Cys mutations in the *α-PheRS* sequence were
494 created by site directed mutagenesis. Like the wild-type cDNA, they were cloned into the
495 *pUASTattB* transformation vector to generate the pUAS-α-PheRS and pUAS-α-PheRS^{Cys}.
496 Before injecting these constructs into fly embryos, all plasmids were verified by sequencing
497 (Microsynth AG, Switzerland). Transgenic flies were generated by applying the *ϕ* C31-based
498 integration system with the stock (*y w att2A[vas-ϕ]; +; attP-86F*) (Bischof et al., 2007).

499 **Western blotting**

500 Protein was extracted from tissues, whole larvae, or flies using the lysis buffer. Protein lysates
501 were separated by SDS-PAGE and transferred onto PVDF membranes (Milipore, US). The
502 blocking was performed for 1h at room temperature (RT) with non-fat dry milk (5%) in TBST
503 solution. Blots were probed first with primary antibodies (diluted in blocking buffer) overnight
504 at 4°C and then with secondary antibodies (diluted in TBST) 1h at RT. The signal of the
505 secondary antibody was detected by using the detect solution mixture (1:1) (ECL™ Prime
506 Western Blotting System, GE Healthcare Life Science) and a luminescent detector (Amersham
507 Imager 600, GE Healthcare Life Science). Origins and recipes of all buffers and reagents are
508 noted in *Key Resource Table*.

509

510 **Immunofluorescent staining and confocal microscopy**

511 Guts were dissected from each female fly 3 days after eclosure, and a total of 10 guts were
512 analyzed for each genotype. Dissections were performed in PBS 1X on ice and tissues were
513 collected within maximum one hour. Fixation with 4% PFA in PBS-T 0.2% at RT was done
514 for different durations depending on the different tissues: two hours (gut), 40 minutes (brain),
515 30 minutes (wing discs, ovary). Then the samples were blocked overnight with blocking buffer
516 at 4°C. Primary antibodies (diluted in blocking buffer) were incubated with the samples for 8h
517 at RT. The samples were rinsed 3 times and washed 3 times (20 minutes/wash) with PBST.
518 Secondary antibodies (diluted in PBST) were incubated overnight at 4°C. The samples were
519 then rinsed 3 times and washed 2 times (20 minutes/wash) with PBST. Hoechst 33258 (2.5
520 µg/ml) was added in PBST before the last washing step and the samples were mounted with
521 Aqua/Poly Mount solution (Polysciences Inc., US). For the anti-Delta labeling, the samples
522 were blocked for 3h at RT with blocking buffer. The primary anti-Delta antibody (1:10 v/v)

523 was incubated with the samples overnight at 4°C and then the secondary antibody was
524 incubated overnight at 4°C. Origins and diluted concentrations of all buffers and antibodies are
525 noted in *Key Resource Table*.

526

527 **Protein synthesis measurements using the ribopuromycylation method (RPM)**

528 For puromycin labeling experiments, tissues were dissected in Schneider's insect medium
529 (Sigma, US) supplement with 10% fetal calf serum (FCS, Sigma, US) at 25°C. They were then
530 incubated with Schneider's insect medium containing puromycin (5 µg/ml, Sigma, US) and
531 cycloheximine (CHX, 100 µg/ml, Sigma, US) for 2 hours at RT. Then the samples were fixed
532 with 4% PFA in PBS-T 0.2% at RT and blocked overnight with blocking buffer at 4°C. Primary
533 anti-Puromycin antibody (diluted in PBST) was incubated with the samples for 8h at RT. The
534 samples were rinsed 3 times and washed 3 times (20 minutes/wash) with PBST. Secondary
535 antibodies (diluted in PBST) were incubated overnight at 4°C. The samples were then rinsed 3
536 times and washed 2 times (20 minutes/wash) with PBST. Hoechst 33258 (2.5 µg/ml) was added
537 in PBST before the last washing step and the samples were mounted with Aqua/Poly Mount
538 solution (Polysciences Inc., US).

539

540 ***In vitro* aminoacylation assay**

541 Recombinant α-PheRS and β-PheRS proteins were expressed in the *E. coli* strain Rosetta
542 (Novagen) and then purified (Moor et al., 2002). For this, the *α-PheRS* or *α-PheR*^{Cys} mutant
543 cDNAs were cloned with His tags at the N-terminal end into the pET-28a plasmid expression
544 vector (Novagen). Wild-type *β-PheRS* cDNAs were cloned into the pET LIC (2A-T) plasmid
545 (Addgene). Then, His-α-PheRS or the His-α-PheR^{Cys} mutant and β-PheRS were co-expressed

546 in the *E. coli* strain Rosetta with isopropylthiogalactoside (IPTG, 1mM) induction at 25 °C for
547 6 hours. Proteins were purified with Ni-NTA affinity resin (Qiagen). The aminoacylation assay
548 protocol from Jiongming Lu was then followed (Lu et al., 2014). This assay was performed at
549 25 °C in a 100µl reaction mixture containing 50 mM Tris-HCl pH 7.5, 10 mM $MgCl_2$, 4 mM
550 ATP, 5 mM β-mercaptoethanol, 100 µg/ml BSA, 3 U/ml *E. coli* carrier tRNA, 5 µM [^{3}H]-
551 amino acid (L-Phe) and 1 µM $tRNA^{Phe}$ from brewer's yeast (Sigma, US). In each experiment,
552 a 15-µl aliquot was removed at four different incubation time points, spotted on a Whatman
553 filter paper discs and washed three times with ice-cold 5% trichloroacetic acid and once with
554 ice-cold ethanol. A blank paper disc without spotting and another with spotting the enzyme-
555 free reaction were used for detecting background signals. After filter discs were dried, they
556 were immersed into PPO Toluol (Sigma, US) solution in plastic bottles and the radioactivity
557 was measured by scintillation counting.

558

559 **Wing disc dissociation and FACS analysis**

560 Wandering larvae derived from 2-4 hours egg collections were dissected in PBS during a
561 maximal time of 30 minutes. Around twenty wing discs were incubated with gentle agitation
562 at 29°C for around 2-hours in 500µl 10× Trypsin-EDTA supplemented with 50 µl 10×Hank's
563 Balanced Salt Solution (HBSS) (Sigma, US) and 10 µl Vybrant DyeCycle Ruby stain
564 (Molecular Probes, US). Dissociated cells from wing discs were directly analyzed by FACS-
565 Calibur flow cytometer (Becton Dickinson, US).

566 *Drosophila* tissue culture cells were harvested and fixed in 70% ethanol and stained
567 with a staining solution containing 1mg/ml propidium iodide, 0.1% Triton and 10 mg/ml RNase
568 A. The cells were then subjected to FACS-Calibur cytometry and data were analyzed with the
569 FlowJo software.

570 ***Drosophila* cell culture and RNAi treatment**

571 The protocols for in vitro cell culture and RNAi treatment was described in the PhD thesis of
572 Jiongming Lu (Lu, 2013). *Drosophila* Kc cells were incubated at 25°C in Schneider's
573 *Drosophila* medium supplemented with 10% heat-inactivated fetal calf serum (FCS) and 50
574 μg/ml Penicillin/Streptomycin. To induce RNAi knockdown in *Drosophila* cells, dsRNA
575 treatment was performed (Clemens et al., 2000). dsRNAs around 500bp in length were
576 generated with the RNAMaxx^{TM} High Yield Transcription Kit (Agilent, US). Cells were
577 diluted to a concentration of 10^6 cells/ml in serum-free medium, and dsRNA was added directly
578 to the medium at a concentration of 15 μg/ml. The cells were incubated for 1 hour followed by
579 addition of medium containing FCS. Then the cells were kept in the incubator and were
580 harvested at different time points (1-5 days) after dsRNA treatment.

581

582 **Clonal assay and twin spot data analysis**

583 For twin spot tests, we used the Mosaic Analysis with a Repressible Cell Marker (MARCM)
584 system. Twin spots were generated with the progenitor genotype *hs-flp; tub-Gal4/UAS-β-*
585 *PheRS ; FRT82B, ubiGFP, UAS-α-PheRS$^{(Cys)}$/FRT82B Tub-Gal80.* In twin spots, the internal
586 control clone was GFP-minus and the sister clone with the red signal generated by the antibody
587 against the overexpressed protein. We induced the *hs-FLP*, *FRT82B* system at 37ºC for 1h on
588 the third day post-eclosure and dissected the animals 3 days post-induction. Confocal imaging
589 detected non-green clones (without ubiGFP) and red clones (stained with Myc antibody-red)
590 (Fig 9A).

591 In twin spots, cell numbers per clone were counted and the numbers of cell division per
592 clone were calculated as $\log_2$(cell numbers per clone). This represents the logarithm of the cell

593 numbers per clone to the base 2. The increase of cell proliferation (%) was analyzed by
594 comparing the number of cell divisions of the two clones in the same twin spot.

595

596 **Image acquisition and processing**

597 Imaging was carried out with a Leica SP8 confocal laser scanning microscope equipped with
598 a 405 nm diode laser, a 458, 476, 488, 496 and 514 nm Argon laser, a 561 nm diode pumped
599 solid state laser and a 633 nm HeNe laser. Images were obtained with 20x dry and 63x oil-
600 immersion objectives and 1024x1024 pixel format. Images were acquired using LAS X
601 software. The images of the entire gut were obtained by imaging at the standard size and then
602 merging maximal projections of Z-stacks with the Tiles Scan tool. Fluorescent intensity was
603 determined from FIJI software.

604

605 **Quantification of cell numbers per posterior midgut**

606 Z stack images through the width of the posterior midgut were acquired along the length of the
607 posterior midgut from the R4a compartment to midgut-hindgut junction. Maximum projections
608 of each Z stack were obtained, and the total number of each cell type was counted manually
609 and exported to Microsoft Excel and GraphPad Prism for further statistical analysis.

610

611 **Quantification and statistical analysis**

612 For quantifications of all experiments, *n* represents the number of independent biological
613 samples analyzed (the number of guts, the number of wing disc, the number of twin spots),
614 error bars represent standard deviation (SD). Statistical significance was determined using the
615 t-test or ANOVA as noted in the figure legends. They were expressed as P values. (*) denotes

616 $p < 0.05$, (**) denotes $p < 0.01$, (***) denotes $p < 0.001$, (****) denotes $p < 0.0001$. (*ns*)
617 denotes values whose difference was not significant.
618
619
620

621 Acknowledgements

622 We thank Peter Nagy, Hugo Stocker, Albena Jordanova, Erik Storkebaum and the
623 Bloomington Stock Center for fly stocks. We are also grateful to Mark Safro for suggesting
624 mutations that disrupt the phenylalanine binding site of α-PheRS. This work was supported
625 by the Novartis Foundation for Medical-Biological Research (#18A050), the Swiss National
626 Fund (project grant 31003A_173188) and the University/Canton of Bern.
627
628

629 Author contributions

630 T.H., J.L. and B.S. conceived the ideas and designed the experiments. T.H. conducted most
631 experiments and performed the analysis of the results. J.L. performed the loss-of-function
632 experiments of PheRS and the mTOR signaling tests, the adult wing measurements and the
633 FACS analysis, including analyzing their data. T.H., J.L. and B.S. wrote the manuscript.
634
635

636 Conflict of interests

637 The authors declare that they have no conflict of interest.

638 # References

639 Ables, J.L., Breunig, J.J., Eisch, A.J., Rakic, P., 2011. Not(ch) just development: Notch
640 signalling in the adult brain. Nature reviews. Neuroscience 12, 269-283.

641 Adam, I., Dewi, D.L., Mooiweer, J., Sadik, A., Mohapatra, S.R., Berdel, B., Keil, M., Sonner,
642 J.K., Thedieck, K., Rose, A.J., Platten, M., Heiland, I., Trump, S., Opitz, C.A., 2018.
643 Upregulation of tryptophanyl-tRNA synthethase adapts human cancer cells to nutritional
644 stress caused by tryptophan degradation. Oncoimmunology 7, e1486353.

645 Antonellis, A., Oprescu, S.N., Griffin, L.B., Heider, A., Amalfitano, A., Innis, J.W., 2018.
646 Compound heterozygosity for loss-of-function FARSB variants in a patient with classic
647 features of recessive aminoacyl-tRNA synthetase-related disease. Human mutation 39, 834-
648 840.

649 Bach, E.A., Ekas, L.A., Ayala-Camargo, A., Flaherty, M.S., Lee, H., Perrimon, N., Baeg,
650 G.H., 2007. GFP reporters detect the activation of the Drosophila JAK/STAT pathway in
651 vivo. Gene expression patterns : GEP 7, 323-331.

652 Barker, N., Ridgway, R.A., van Es, J.H., van de Wetering, M., Begthel, H., van den Born, M.,
653 Danenberg, E., Clarke, A.R., Sansom, O.J., Clevers, H., 2009. Crypt stem cells as the cells-
654 of-origin of intestinal cancer. Nature 457, 608-611.

655 Bina, S., Wright, V.M., Fisher, K.H., Milo, M., Zeidler, M.P., 2010. Transcriptional targets of
656 Drosophila JAK/STAT pathway signalling as effectors of haematopoietic tumour formation.
657 EMBO reports 11, 201-207.

658 Bischof, J., Maeda, R.K., Hediger, M., Karch, F., Basler, K., 2007. An optimized transgenesis
659 system for Drosophila using germ-line-specific phiC31 integrases. Proceedings of the
660 National Academy of Sciences of the United States of America 104, 3312-3317.

661 Bonfils, G., Jaquenoud, M., Bontron, S., Ostrowicz, C., Ungermann, C., De Virgilio, C.,
662 2012. Leucyl-tRNA synthetase controls TORC1 via the EGO complex. Molecular cell 46,
663 105-110.

664 Buchon, N., Broderick, N.A., Chakrabarti, S., Lemaitre, B., 2009. Invasive and indigenous
665 microbiota impact intestinal stem cell activity through multiple pathways in Drosophila.
666 Genes & development 23, 2333-2344.

667 Casas-Tinto, S., Lolo, F.N., Moreno, E., 2015. Active JNK-dependent secretion of
668 Drosophila Tyrosyl-tRNA synthetase by loser cells recruits haemocytes during cell
669 competition. Nature communications 6, 10022.

670 Chen, J., Larochelle, S., Li, X., Suter, B., 2003. Xpd/Ercc2 regulates CAK activity and
671 mitotic progression. Nature 424, 228-232.

672 Clemens, J.C., Worby, C.A., Simonson-Leff, N., Muda, M., Maehama, T., Hemmings, B.A.,
673 Dixon, J.E., 2000. Use of double-stranded RNA interference in Drosophila cell lines to
674 dissect signal transduction pathways. Proceedings of the National Academy of Sciences 97,
675 6499-6503.

676 de la Pompa, J.L., Wakeham, A., Correia, K.M., Samper, E., Brown, S., Aguilera, R.J.,
677 Nakano, T., Honjo, T., Mak, T.W., Rossant, J., Conlon, R.A., 1997. Conservation of the
678 Notch signalling pathway in mammalian neurogenesis. Development 124, 1139-1148.

679 Deliu, L.P., Ghosh, A., Grewal, S.S., 2017. Investigation of protein synthesis in Drosophila
680 larvae using puromycin labelling. Biology open 6, 1229-1234.

681 Dolde, C., Lu, J., Suter, B., 2014. Cross Talk between Cellular Regulatory Networks
682 Mediated by Shared Proteins. Advances in Biology 2014, 12.

683 Finarov, I., Moor, N., Kessler, N., Klipcan, L., Safro, M.G., 2010. Structure of human
684 cytosolic phenylalanyl-tRNA synthetase: evidence for kingdom-specific design of the active
685 sites and tRNA binding patterns. Structure 18, 343-353.

686 Giachino, C., Taylor, V., 2014. Notching up neural stem cell homogeneity in homeostasis and
687 disease. Frontiers in neuroscience 8, 32.

688 Gomard-Mennesson, E., Fabien, N., Cordier, J.F., Ninet, J., Tebib, J., Rousset, H., 2007.
689 Clinical significance of anti-histidyl-tRNA synthetase (Jo1) autoantibodies. Annals of the
690 New York Academy of Sciences 1109, 414-420.

691 Grandbarbe, L., Bouissac, J., Rand, M., Hrabe de Angelis, M., Artavanis-Tsakonas, S.,
692 Mohier, E., 2003. Delta-Notch signaling controls the generation of neurons/glia from neural
693 stem cells in a stepwise process. Development 130, 1391-1402.

694 Greenberg, Y., King, M., Kiosses, W.B., Ewalt, K., Yang, X., Schimmel, P., Reader, J.S.,
695 Tzima, E., 2008. The novel fragment of tyrosyl tRNA synthetase, mini-TyrRS, is secreted to
696 induce an angiogenic response in endothelial cells. FASEB journal : official publication of
697 the Federation of American Societies for Experimental Biology 22, 1597-1605.

698 Guo, M., Schimmel, P., 2013. Essential nontranslational functions of tRNA synthetases.
699 Nature chemical biology 9, 145-153.

700 Han, J.M., Jeong, S.J., Park, M.C., Kim, G., Kwon, N.H., Kim, H.K., Ha, S.H., Ryu, S.H.,
701 Kim, S., 2012. Leucyl-tRNA synthetase is an intracellular leucine sensor for the mTORC1-
702 signaling pathway. Cell 149, 410-424.

703 Hariharan, I.K., 2015. Organ Size Control: Lessons from Drosophila. Developmental cell 34,
704 255-265.

705 Hatakeyama, J., Bessho, Y., Katoh, K., Ookawara, S., Fujioka, M., Guillemot, F., Kageyama,
706 R., 2004. Hes genes regulate size, shape and histogenesis of the nervous system by control of
707 the timing of neural stem cell differentiation. Development 131, 5539-5550.

708 Herrera, S.C., Bach, E.A., 2019. JAK/STAT signaling in stem cells and regeneration: from
709 Drosophila to vertebrates. Development 146.

710 Housden, B.E., Millen, K., Bray, S.J., 2012. Drosophila Reporter Vectors Compatible with
711 PhiC31 Integrase Transgenesis Techniques and Their Use to Generate New Notch Reporter
712 Fly Lines. G3 (Bethesda) 2, 79-82.

713 Jiang, H., Patel, P.H., Kohlmaier, A., Grenley, M.O., McEwen, D.G., Edgar, B.A., 2009.
714 Cytokine/Jak/Stat signaling mediates regeneration and homeostasis in the Drosophila midgut.
715 Cell 137, 1343-1355.

716 Kim, D., Kwon, N.H., Kim, S., 2014. Association of aminoacyl-tRNA synthetases with
717 cancer. Topics in current chemistry 344, 207-245.

718 Ko, Y.G., Kang, Y.S., Kim, E.K., Park, S.G., Kim, S., 2000. Nucleolar localization of human
719 methionyl-tRNA synthetase and its role in ribosomal RNA synthesis. The Journal of cell
720 biology 149, 567-574.

721 Ko, Y.G., Kim, E.Y., Kim, T., Park, H., Park, H.S., Choi, E.J., Kim, S., 2001. Glutamine-
722 dependent antiapoptotic interaction of human glutaminyl-tRNA synthetase with apoptosis
723 signal-regulating kinase 1. The Journal of biological chemistry 276, 6030-6036.

724 Koch, R., Ledermann, R., Urwyler, O., Heller, M., Suter, B., 2009. Systematic functional
725 analysis of Bicaudal-D serine phosphorylation and intragenic suppression of a female sterile
726 allele of BicD. PloS one 4, e4552.

727 Korzelius, J., Naumann, S.K., Loza-Coll, M.A., Chan, J.S., Dutta, D., Oberheim, J., Glasser,
728 C., Southall, T.D., Brand, A.H., Jones, D.L., Edgar, B.A., 2014. Escargot maintains stemness
729 and suppresses differentiation in Drosophila intestinal stem cells. The EMBO journal 33,
730 2967-2982.

731 Laplante, M., Sabatini, D.M., 2012. mTOR signaling in growth control and disease. Cell 149,
732 274-293.

733 Lee, S.W., Cho, B.H., Park, S.G., Kim, S., 2004. Aminoacyl-tRNA synthetase complexes:
734 beyond translation. Journal of cell science 117, 3725-3734.

735 Lin, G., Xu, N., Xi, R., 2010. Paracrine unpaired signaling through the JAK/STAT pathway
736 controls self-renewal and lineage differentiation of drosophila intestinal stem cells. Journal of
737 molecular cell biology 2, 37-49.

738 Ling, J., Yadavalli, S.S., Ibba, M., 2007. Phenylalanyl-tRNA synthetase editing defects result
739 in efficient mistranslation of phenylalanine codons as tyrosine. RNA 13, 1881-1886.

740 Lu, J., 2013. Phenylalanyl tRNA synthetase: functions in and beyond aminoacylation,
741 Institute of Cell Biology. University of Bern, Bern, Switzerland.

742 Lu, J., Bergert, M., Walther, A., Suter, B., 2014. Double-sieving-defective aminoacyl-tRNA
743 synthetase causes protein mistranslation and affects cellular physiology and development.
744 Nature communications 5, 5650.

745 Markowitz, S.D., Bertagnolli, M.M., 2009. Molecular origins of cancer: Molecular basis of
746 colorectal cancer. The New England journal of medicine 361, 2449-2460.

747 Martin, F.A., Morata, G., 2006. Compartments and the control of growth in the Drosophila
748 wing imaginal disc. Development 133, 4421-4426.

749 Micchelli, C.A., Perrimon, N., 2006. Evidence that stem cells reside in the adult Drosophila
750 midgut epithelium. Nature 439, 475-479.

751 Moor, N., Linshiz, G., Safro, M., 2002. Cloning and expression of human phenylalanyl-tRNA
752 synthetase in Escherichia coli: comparative study of purified recombinant enzymes. Protein
753 expression and purification 24, 260-267.

754 Muller, P., Kuttenkeuler, D., Gesellchen, V., Zeidler, M.P., Boutros, M., 2005. Identification
755 of JAK/STAT signalling components by genome-wide RNA interference. Nature 436, 871-
756 875.

757 Nathanson, L., Deutscher, M.P., 2000. Active aminoacyl-tRNA synthetases are present in
758 nuclei as a high molecular weight multienzyme complex. The Journal of biological chemistry
759 275, 31559-31562.

760 Niehues, S., Bussmann, J., Steffes, G., Erdmann, I., Kohrer, C., Sun, L., Wagner, M.,
761 Schafer, K., Wang, G., Koerdt, S.N., Stum, M., Jaiswal, S., RajBhandary, U.L., Thomas, U.,
762 Aberle, H., Burgess, R.W., Yang, X.L., Dieterich, D., Storkebaum, E., 2015. Impaired protein
763 translation in Drosophila models for Charcot-Marie-Tooth neuropathy caused by mutant
764 tRNA synthetases. Nature communications 6, 7520.

765 Ohlstein, B., Spradling, A., 2007. Multipotent Drosophila intestinal stem cells specify
766 daughter cell fates by differential notch signaling. Science 315, 988-992.

767 Otani, A., Slike, B.M., Dorrell, M.I., Hood, J., Kinder, K., Ewalt, K.L., Cheresh, D.,
768 Schimmel, P., Friedlander, M., 2002. A fragment of human TrpRS as a potent antagonist of
769 ocular angiogenesis. Proceedings of the National Academy of Sciences of the United States
770 of America 99, 178-183.

771 Patel, P.H., Dutta, D., Edgar, B.A., 2015. Niche appropriation by Drosophila intestinal stem
772 cell tumours. Nature cell biology 17, 1182-1192.

773 Qiao, L., Wong, B.C., 2009. Role of Notch signaling in colorectal cancer. Carcinogenesis 30,
774 1979-1986.

775 Roy, H., Ibba, M., 2006. Phenylalanyl-tRNA synthetase contains a dispensable RNA-binding
776 domain that contributes to the editing of noncognate aminoacyl-tRNA. Biochemistry 45,
777 9156-9162.

778 Schimmel, P.R., Soll, D., 1979. Aminoacyl-tRNA synthetases: general features and
779 recognition of transfer RNAs. Annual review of biochemistry 48, 601-648.

780 Sen, S., Zhou, H., Ripmaster, T., Hittelman, W.N., Schimmel, P., White, R.A., 1997.
781 Expression of a gene encoding a tRNA synthetase-like protein is enhanced in tumorigenic
782 human myeloid leukemia cells and is cell cycle stage- and differentiation-dependent.
783 Proceedings of the National Academy of Sciences of the United States of America 94, 6164-
784 6169.

785 Smirnova, E.V., Lakunina, V.A., Tarassov, I., Krasheninnikov, I.A., Kamenski, P.A., 2012.
786 Noncanonical functions of aminoacyl-tRNA synthetases. Biochemistry. Biokhimiia 77, 15-
787 25.

788 Takashima, S., Adams, K.L., Ortiz, P.A., Ying, C.T., Moridzadeh, R., Younossi-Hartenstein,
789 A., Hartenstein, V., 2011. Development of the Drosophila entero-endocrine lineage and its
790 specification by the Notch signaling pathway. Developmental biology 353, 161-172.

791 Tzima, E., Reader, J.S., Irani-Tehrani, M., Ewalt, K.L., Schwartz, M.A., Schimmel, P., 2005.
792 VE-cadherin links tRNA synthetase cytokine to anti-angiogenic function. The Journal of
793 biological chemistry 280, 2405-2408.

794 Wang, C., Guo, X., Dou, K., Chen, H., Xi, R., 2015. Ttk69 acts as a master repressor of
795 enteroendocrine cell specification in Drosophila intestinal stem cell lineages. Development
796 142, 3321-3331.

797 Wang, H., Chen, X., He, T., Zhou, Y., Luo, H., 2013. Evidence for tissue-specific Jak/STAT
798 target genes in Drosophila optic lobe development. Genetics 195, 1291-1306.

799 Wu, J.S., Luo, L., 2006. A protocol for mosaic analysis with a repressible cell marker
800 (MARCM) in Drosophila. Nature protocols 1, 2583-2589.

801 Wullschleger, S., Loewith, R., Hall, M.N., 2006. TOR signaling in growth and metabolism.
802 Cell 124, 471-484.

803 Yannay-Cohen, N., Carmi-Levy, I., Kay, G., Yang, C.M., Han, J.M., Kemeny, D.M., Kim,
804 S., Nechushtan, H., Razin, E., 2009. LysRS serves as a key signaling molecule in the immune
805 response by regulating gene expression. Molecular cell 34, 603-611.

806 Yin, C., Xi, R., 2018. A Phyllopod-Mediated Feedback Loop Promotes Intestinal Stem Cell
807 Enteroendocrine Commitment in Drosophila. Stem cell reports 10, 43-57.

808 Yin, L., Velazquez, O.C., Liu, Z.J., 2010. Notch signaling: emerging molecular targets for
809 cancer therapy. Biochemical pharmacology 80, 690-701.

810 Zhou, J.J., Wang, F., Xu, Z., Lo, W.S., Lau, C.F., Chiang, K.P., Nangle, L.A., Ashlock,
811 M.A., Mendlein, J.D., Yang, X.L., Zhang, M., Schimmel, P., 2014. Secreted histidyl-tRNA
812 synthetase splice variants elaborate major epitopes for autoantibodies in inflammatory
813 myositis. The Journal of biological chemistry 289, 19269-19275.

814

815

816 # Figure legends:

817

818 **Figure 1: *α–PheRS* overexpression increases numbers of mitotic cells without stimulating**
819 **translation.**

820 (A-B'''',C) Wing disc phenotypes induced by the overexpression of α-*PheRS* or α-*PheRS*^{Cys}. *en-Gal4*
821 was used to drive transgene expression in the posterior compartment of developing wing discs. Mitotic
822 cells were labelled with anti-phospho-Histone H3 (PH3) antibodies (A: anterior compartment; P:
823 posterior compartment). n=10, *p<0.05, **p<0.01 in t-test. (D-E'',F) Protein synthesis did not increase
824 upon overexpression of *α-PheRS* or *α-PheRS* and *β-PheRS* together. *en-Gal4* was used to drive the
825 overexpression of the transgenes in the posterior compartment of wing discs. dMyc was used as
826 positive control. Protein synthesis was measured by the mean intensity of the puromycin (PMY) signal
827 labelling the nascent polypeptides. n=15, ****p<0.0001, *ns:* not significant.

828

829 **Figure 2: PheRS overexpression in wing discs induces excessive cell growth.**

830 (A,B) PheRS overexpression increases wing size. One wing was chosen from each female fly, and a
831 total of 20 wings were analyzed for each genotype. Quantification of wing size was performed by
832 counting the pixels in both anterior (A) and posterior (P) compartments of the wing and calculating
833 their ratio (P/A). PheRS overexpression of both subunits, but not a single subunit alone, increases
834 wing size. GlyRS overexpression did not increase wing size, but slightly decreased it. Note that only
835 the upper section of the y axis is shown. n=20, **, p<0.01 in t-test.

836

837 **Figure 3: The proliferative activity of the *α-PheRS* subunit is independent of PheRS complex**
838 **formation and tRNA^{Phe} aminoacylation.**

839 Clonal analysis (twin spot) experiment of the effect of overexpression of the PheRS subunits in follicle
840 cells by the MARCM technique. After inducing mitotic recombination by expressing the flippase
841 under the control of the heat-shock (*hs*) promoter at 37ºC for 40 minutes, a recombining cell will
842 divide and give rise to two proliferating clones. (A) One clone (red) overexpresses PheRS and its twin
843 clone (GFP^- signal) does not and expresses normal levels (internal control, outlined with yellow line).
844 (B) Three days after inducing the recombination, the average number of cell divisions were calculated
845 for each clone and compared to its twin spot to obtain the proliferation increase (%). n= 30, **p<0.01,
846 ***p<0.001, ****p<0.0001 in ANOVA test.

847

848 **Figure 4: α-PheRS promotes ISC proliferation in the midgut.**

849 (A) The number of ISC clusters increased upon overexpression of *Myc::α-PheRS* in ISCs and EBs
850 (Esg^+-cells) of the larval gut. n=10, *p<0.05,****p<0.0001. (B) The cell number per Esg^+ cluster
851 increased upon overexpression of *Myc::α-PheRS* with the same *esg-Gal4* driver used in (A). Esg^+
852 clusters were categorized according to the number of cells per cluster. The fraction of big clusters (cell
853 number > 5) increased upon overexpression of *Myc::α-PheRS.* In contrast, the overexpression of *β-*
854 *PheRS::V5* alone or the overexpression of *β-PheRS::V5* together with *Myc::α-PheRS* showed the
855 same frequency of the different clusters as the wild type. (C-G) Whole gut images and pictures of the
856 posterior midgut area (C'-G') showing the different cells observed. The expression of the different
857 genes indicated were driven with the same driver used in (A). The eYFP signal (YFP) displayed in
858 green marks ISCs and EBs, Hoechst (blue) stains the DNA in the nuclei. Overexpression of the *α-*
859 $PheRS^{Cys}$ mutant gave rise to tumor-like areas in both the anterior and the posterior midgut (outlined
860 with dashed lines). (H) Mitotic cells were labelled with anti-phospho-Histone H3 (PH3) antibodies.
861 n=10, ****p<0.0001 in t-test. (I) Total cells per intestinal region were measured by counting Hoechst
862 33258 labeled cells manually. n=10, ****p<0.0001. (J-J") The overexpression of *α-PheRS* or *α-*
863 $PheRS^{Cys}$ with the *esg-Gal4* driver in adult guts also resulted in an over-proliferation phenotype of
864 Esg^+ stem cells and progenitor cells.

865

866 **Figure 5: Elevated α-PheRS levels increase EE differentiation in the gut through**
867 **downregulating Notch signaling.**

868 (A-B,C) Overexpression of *α-PheRS*^{Cys} using the *esg-Gal4,UAS-2XEYFP* system led to an increase in
869 the number of EEs compared to the ECs in both larval and adult guts. EEs were marked by anti-
870 Prospero antibody, Hoechst-labelled polyploid cells were counted as ECs. Guts were dissected from
871 female flies 3 days after eclosure, and at least 10 guts were analyzed for each genotype. n=10,
872 ****p<0.0001. (A",B") The co-overexpression of *α-PheRS*^{Cys} with *Notch* rescued the over-
873 proliferation of Esg^{+} cells as well as the EE/EC ratio.

874 (D-E') Whole adult gut images (D,E) and the posterior midgut area (D',E'). The same *esg-Gal4* driver
875 marks ISCs and EBs (eYFP signal shown in green), Hoechst (blue) stains nuclear DNA. The *Notch*
876 knockdown phenotype in the posterior midgut (outlined with dashed lines) is indistinguishable from
877 the *α-PheRS*^{Cys} overexpression phenotype. Co-overexpression of *α-PheRS*^{Cys} with *Notch* rescued the
878 midgut phenotype. (F) Notch activity reporter (NRE-EGFP) levels drastically decrease upon *α-PheRS*
879 or *α-PheRS*^{Cys} overexpression in adult midgut ISCs that expresses GFP under the control of a Notch
880 response element (NRE). The guts were dissected from female flies 3 days after eclosure. Protein
881 lysates were then extracted and separated by SDS-PAGE gel. 25 guts were analyzed for each
882 genotype.

883

884 **Figure 6: High levels of *α-PheRS* repress neuroblast proliferation by downregulating the *Notch***
885 **pathway.**

886 (A-A") The overexpression of *α-PheRS* or *α-PheRS*^{Cys} in neuroblasts reduced the ratio central brain
887 (CB) size to optic lobe (OL) size. The *insc-Gal4,UAS-GFP* system was used to overexpress proteins in
888 neuroblasts (NBs). NBs were labelled by GFP expression. Central brain (right area with GFP^{+} NBs)
889 area is outlined by a white dashed line. (B) Effect of overexpression and knock down of *α-*

890 *PheRS*$^{(Cys)}$and *Notch* on the CB/OL size ratio. n=20, ***p<0.001, *ns*: not significant. (C) The larval
891 brains were dissected from third instar larvae, and at least 20 brains were analyzed for each genotype.
892 Each brain lobe was classified according to the number of type II NBs per brain lobe. The
893 overexpression of *α-PheRS* or *α-PheRS*^{Cys} reduced the number of type II NBs per brain lobe, and less
894 than half of the lobes contained the normal 7-8 NBs. *Notch RNAi* caused the same phenotype with
895 higher expressivity. Overexpressing *Notch* together with *α-PheRS*^{Cys} rescued the loss of NB phenotype
896 to normal wild-type levels. n = 25.

897

898 **Figure 7: The JAK/STAT transcription factor Stat92E regulates α-PheRS levels.**

899 (A-C'') Hypomorphic *Stat92E*^{HJ} mutants contain high levels of α-PheRS in their ISCs (B). Anti-Delta
900 antibody was used to label ISCs, and anti-α-PheRS was used to stain for α-PheRS. *esg-Gal4,UAS-*
901 *2XEYFP* was used to drive YFP expression (A-A'', control) and *Stat92E* RNAi (C-C''), respectively,
902 in ISCs and EBs. The white arrows indicate polyploid ECs with high levels of α-PheRS. (D-F') The
903 quantification of the signal in the image (A",B",C") is based on the line across the nucleus of the cell.
904 The signal intensity of α-PheRS differs between the ISC/EB (high) and distant EC (low) while the
905 signal intensity of α-PheRS is similar between the ISC/EB (high) and the neighboring EC (high). (G)
906 Suppressing the JAK/STAT signaling with the hypomorphic *Stat92E*^{HJ} allele or by RNAi significantly
907 elevated the levels of α-PheRS in ISCs/EBs and neighboring ECs (Nb EC), but not in distant ECs. α-
908 PheRS levels were measured by the mean intensity of the fluorescent signal. n=10, ****p<0.0001, *ns:*
909 not significant. (H-I'') The overexpression of Stat92E decreased α-PheRS levels in Esg^{+} cells (circled
910 with white dashed lines) in adult guts. The same setting was used as in (A). (J-K''') The *Stat92E*
911 activity did not alter upon overexpression of α-PheRS. The *10X STAT92E-GFP* reporter was used to
912 measure *Stat92E* activity. It expresses GFP under the control of 10 Stat92E binding sites. The *esg-*
913 *Gal4,UAS-mCD8:mCherry,tub-Gal80*^{ts} *system* was used to overexpress *α-PheRS* in ISCs and EBs.
914 The female flies were collected 3 days after eclosure and cultured at 29ºC for 7 days before dissecting
915 and harvesting their midguts.

Figure 1

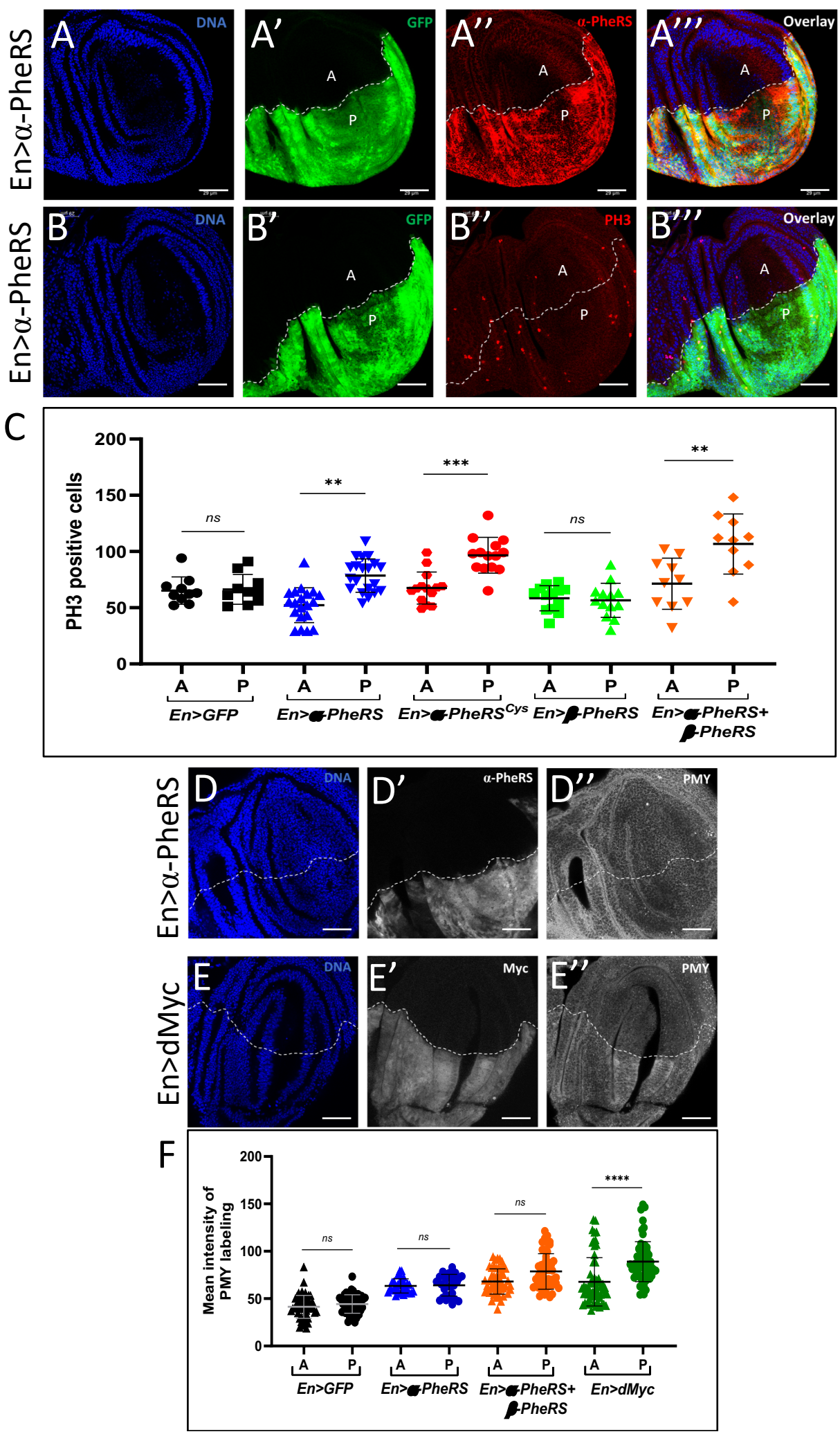
En>α-PheRS
A
DNA
A'
GFP
A''
α-PheRS
A'''
Overlay
A
P
En>α-PheRS
B
DNA
B'
GFP
B''
PH3
B'''
Overlay
C
PH3 positive cells
200
150
100
50
0
ns
**
***
ns
**
A
P
En>GFP
En>α-PheRS
En>α-PheRS^Cys
En>β-PheRS
En>α-PheRS+ β-PheRS
En>α-PheRS
D
DNA
D'
α-PheRS
D''
PMY
En>dMyc
E
DNA
E'
Myc
E''
PMY
F
Mean intensity of PMY labeling
200
150
100
50
0
ns
ns
ns
****
A
P
En>GFP
En>α-PheRS
En>α-PheRS+ β-PheRS
En>dMyc

Figure 2

A

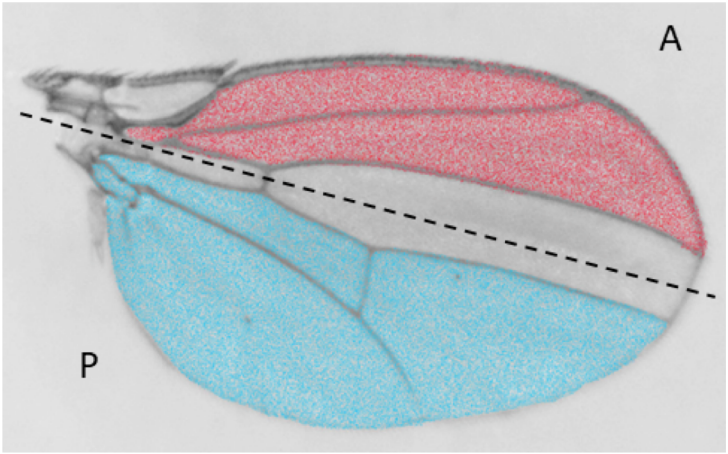
A
P

B

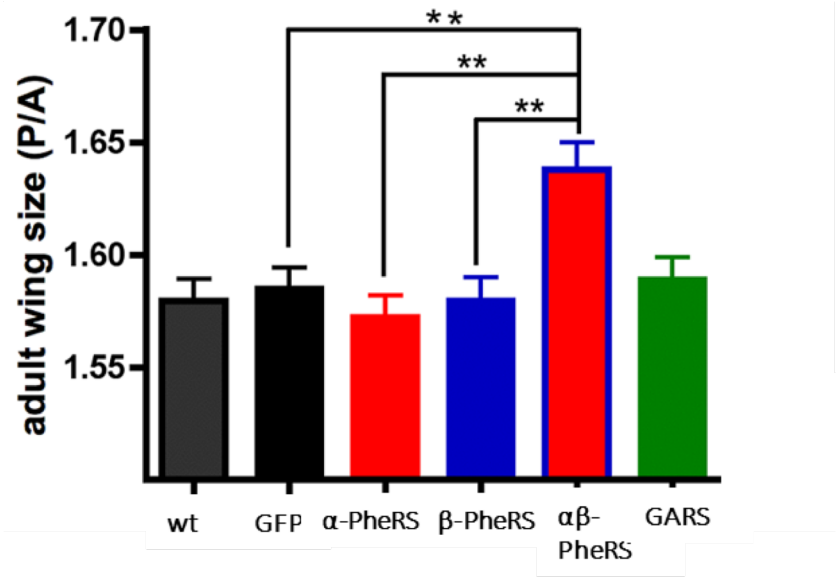
adult wing size (P/A)
1.70
1.65
1.60
1.55
**
**
**
wt
GFP
α-PheRS
β-PheRS
αβ-PheRS
GARS

Figure 3

A

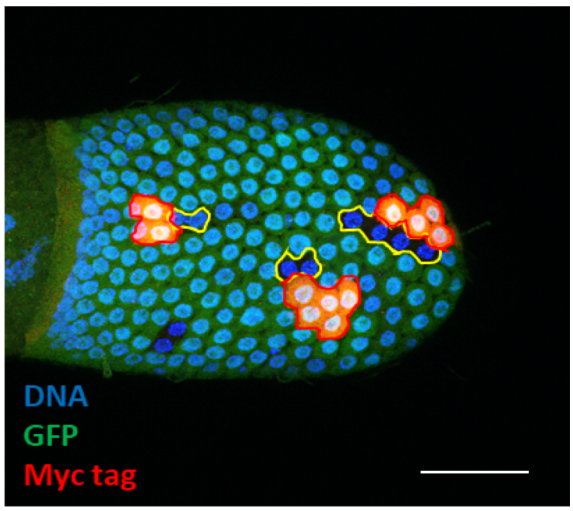
DNA
GFP
Myc tag

B

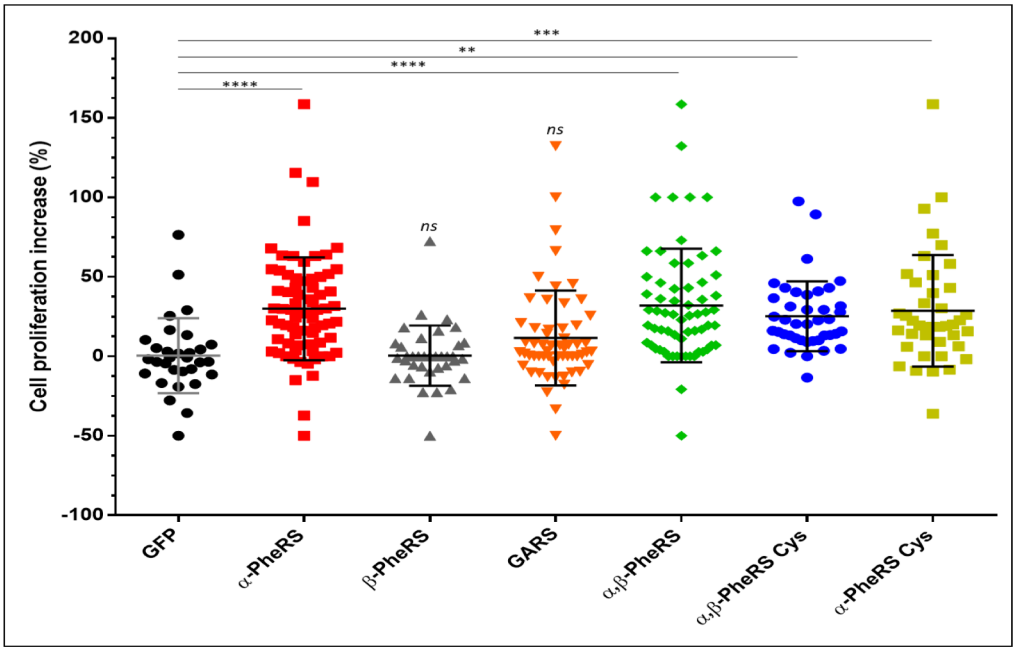
Cell proliferation increase (%)
200
150
100
50
0
-50
-100
***
**
****
****
ns
ns
GFP
α-PheRS
β-PheRS
GARS
α,β-PheRS
α,β-PheRS Cys
α-PheRS Cys

Figure 4

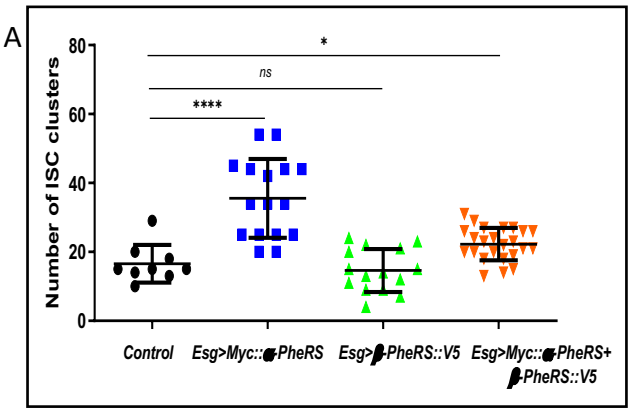

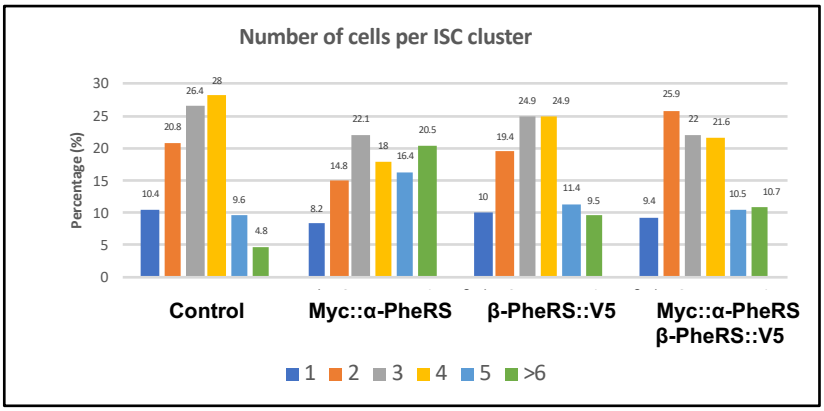

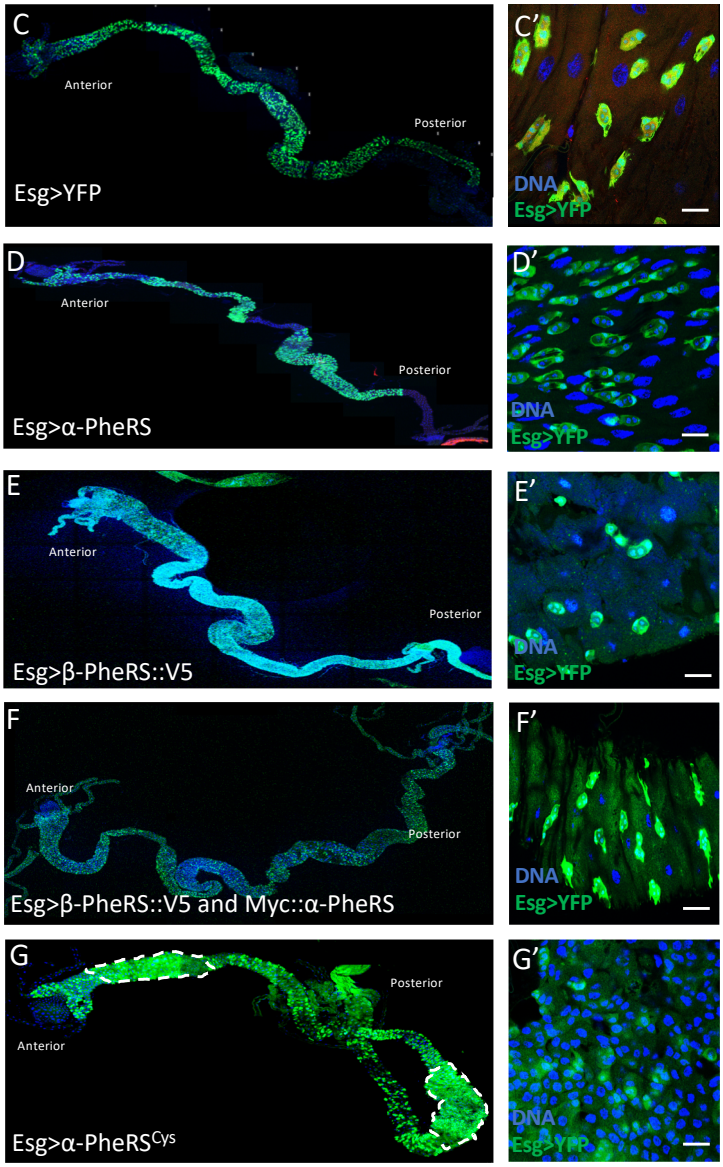

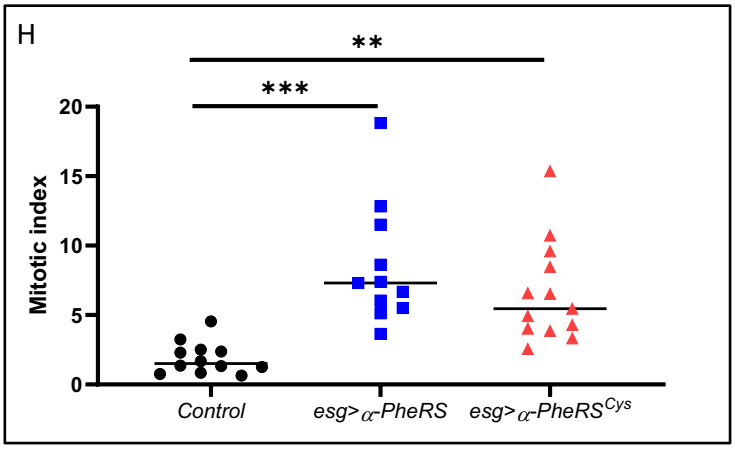

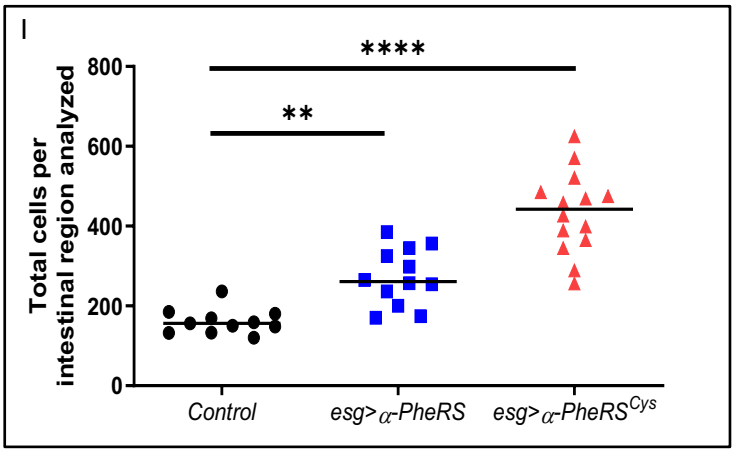

Adult midgut

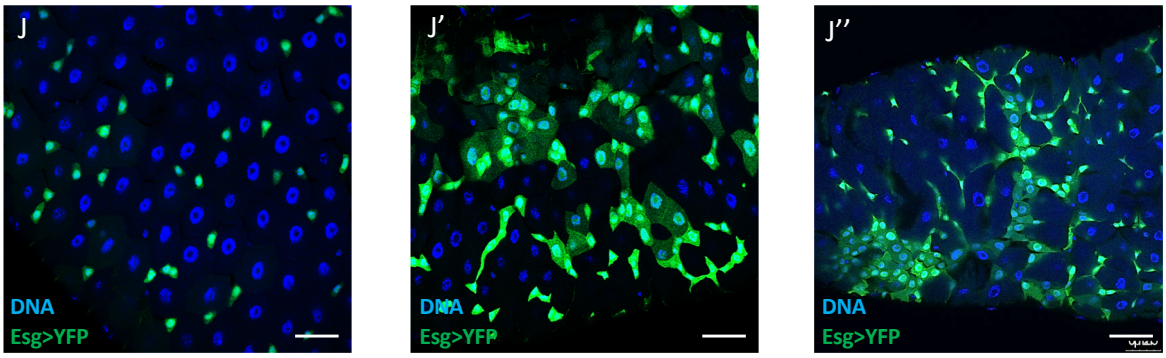

Figure 5

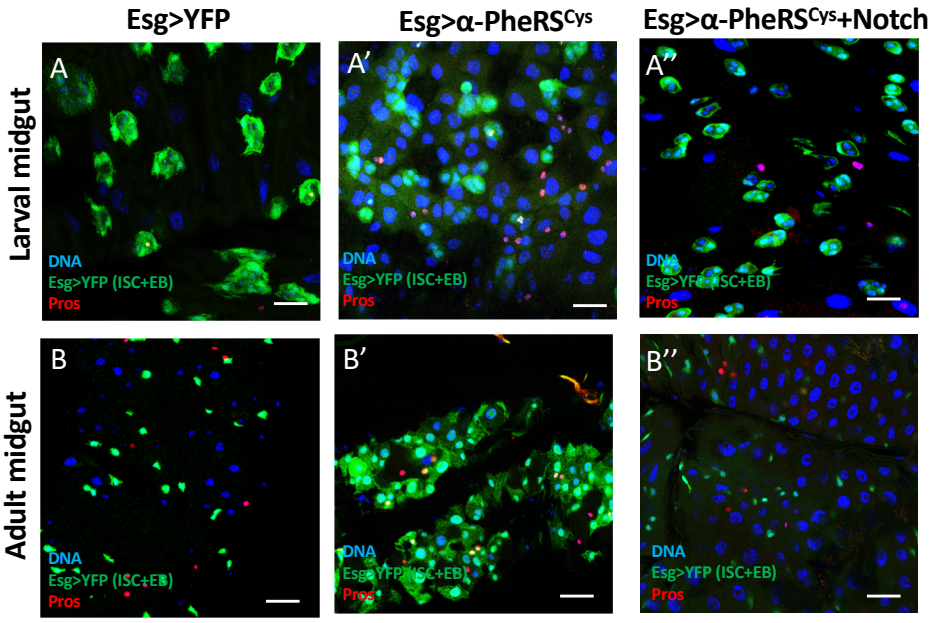
Esg>YFP
Esg>α-PheRS^Cys
Esg>α-PheRS^Cys+Notch
Larval midgut
Adult midgut
A
A'
A''
B
B'
B''
DNA
Esg>YFP (ISC+EB)
Pros

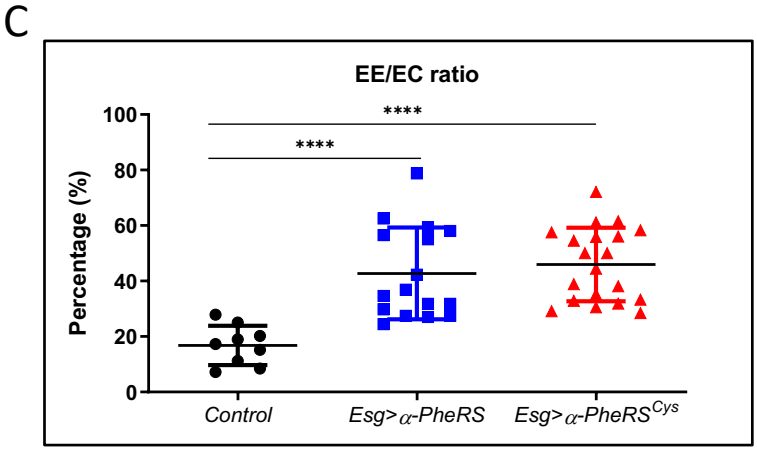
C
EE/EC ratio
Percentage (%)
100
80
60
40
20
0
****
****
Control
Esg>α-PheRS
Esg>α-PheRS^Cys

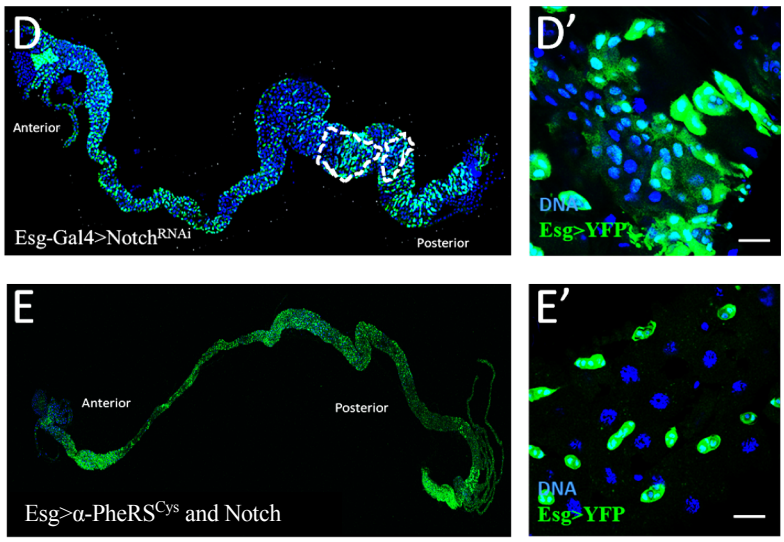
D
Anterior
Posterior
Esg-Gal4>Notch^RNAi
D'
DNA
Esg>YFP
E
Anterior
Posterior
Esg>α-PheRS^Cys and Notch
E'
DNA
Esg>YFP

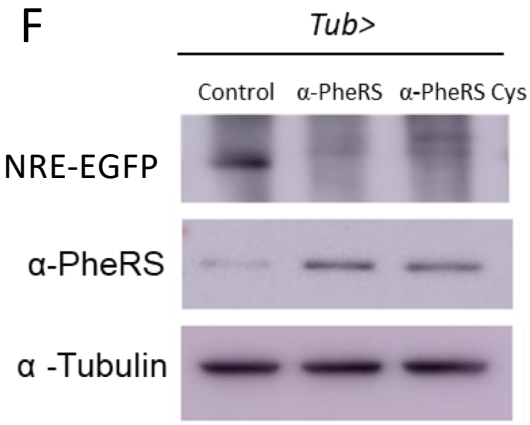
F
Tub>
Control
α-PheRS
α-PheRS Cys
NRE-EGFP
α-PheRS
α -Tubulin

Figure 6

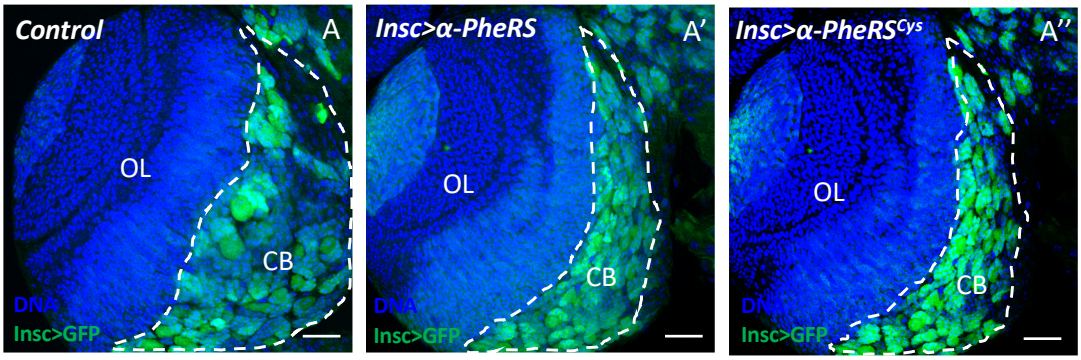
Control
A
OL
CB
DNA
Insc>GFP
Insc>α-PheRS
A'
OL
CB
DNA
Insc>GFP
Insc>α-PheRSCys
A''
OL
CB
DNA
Insc>GFP

B

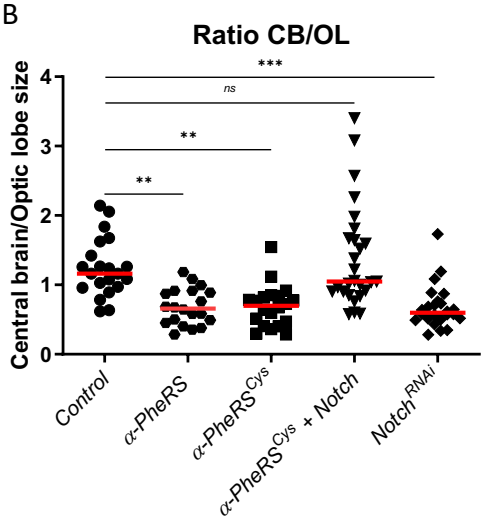
Ratio CB/OL
Central brain/Optic lobe size
0
1
2
3
4
***
ns
**
**
Control
α-PheRS
α-PheRSCys
α-PheRSCys + Notch
NotchRNAi

C

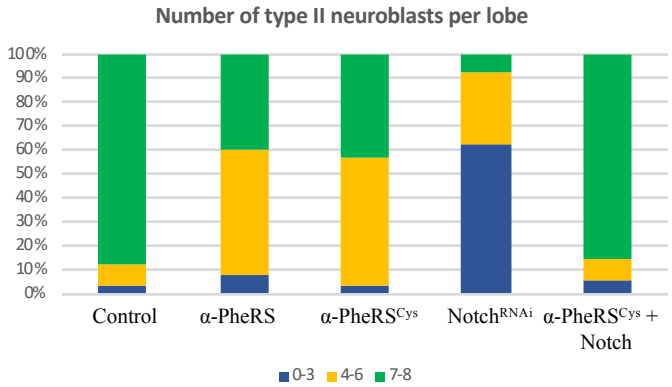
Number of type II neuroblasts per lobe
100%
90%
80%
70%
60%
50%
40%
30%
20%
10%
0%
Control
α-PheRS
α-PheRSCys
NotchRNAi
α-PheRSCys + Notch
0-3
4-6
7-8

Figure 7

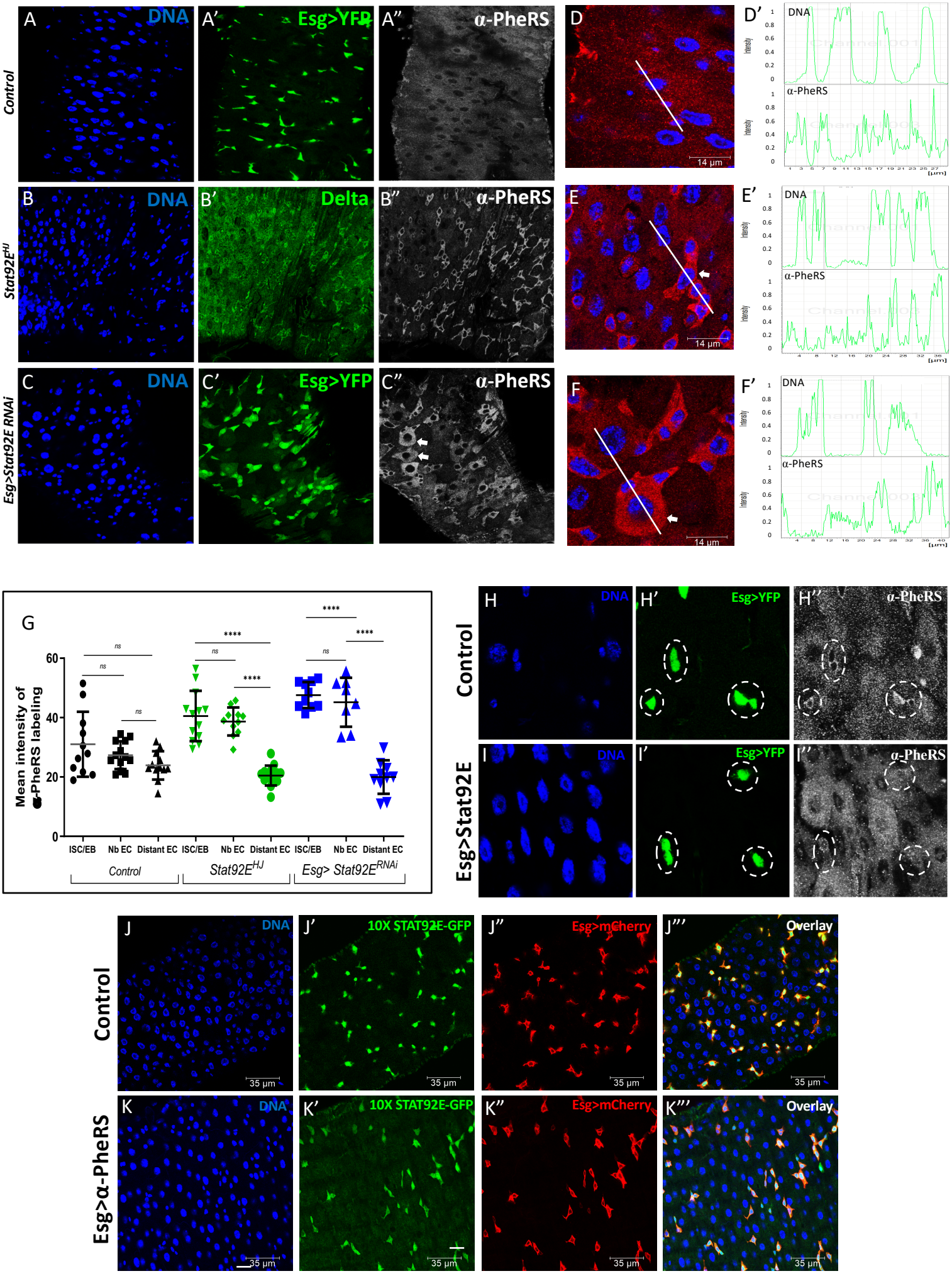
A
DNA
A'
Esg>YFP
A"
α-PheRS
Control
B
DNA
B'
Delta
B"
α-PheRS
Stat92E^HJ
C
DNA
C'
Esg>YFP
C"
α-PheRS
Esg>Stat92E RNAi
D
14 µm
D'
DNA
α-PheRS
Intensity
E
14 µm
E'
DNA
α-PheRS
F
14 µm
F'
DNA
α-PheRS
G
Mean intensity of α-PheRS labeling
ISC/EB
Nb EC
Distant EC
Control
Stat92E^HJ
Esg> Stat92E^RNAi
ns
****
H
DNA
H'
Esg>YFP
H"
α-PheRS
Control
I
DNA
I'
Esg>YFP
I"
α-PheRS
Esg>Stat92E
J
DNA
J'
10X STAT92E-GFP
J"
Esg>mCherry
J'''
Overlay
Control
K
DNA
K'
10X STAT92E-GFP
K"
Esg>mCherry
K'''
Overlay
Esg>α-PheRS
35 µm

Supplementary Figure S1

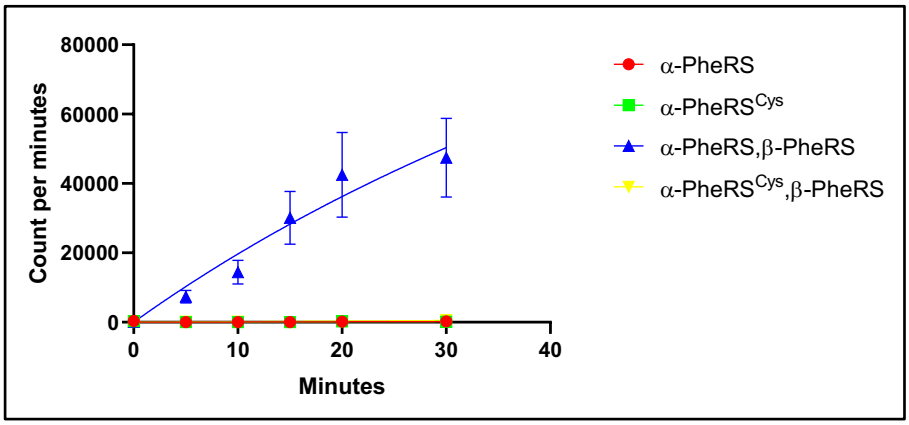

Figure S1:
The *α–PheRS^{Cys}* mutant does not support aminoacylation in vitro. The aminoacylation assay was performed with the mixture of the recombinant protein (α–PheRS or α–PheRS^{Cys} and β-PheRS) produced in E. coli. tRNA^{Phe} from yeast was aminoacylated with [^{3}H] phenylalanine. The [^{3}H] phenylalanine signal coupled with tRNA^{Phe} was counted by the scintillation counter. CPM= counts per minute.

Supplementary Figure S2

Analyzing the size of dissociated larval wing disc cells by FACS revealed that the cells from the posterior compartment (GFP-positive compartment), where both PheRS subunits were overexpressed, were on average larger than the ones that overexpressed only GFP or only α-PheRS (A). In contrast, all control cells from the anterior (GFP-negative) compartment of these three lines were of similar, smaller size (A). Cell numbers, on the other hand, did not significantly change upon overexpression of both PheRS subunits (B). We conclude that in larval wing discs with their organ size control mechanism, PheRS overexpression causes primarily an increase in cell size. On the other hand, single overexpression of α-PheRS increases the mitotic index of wing discs (Fig 1A-C).

A

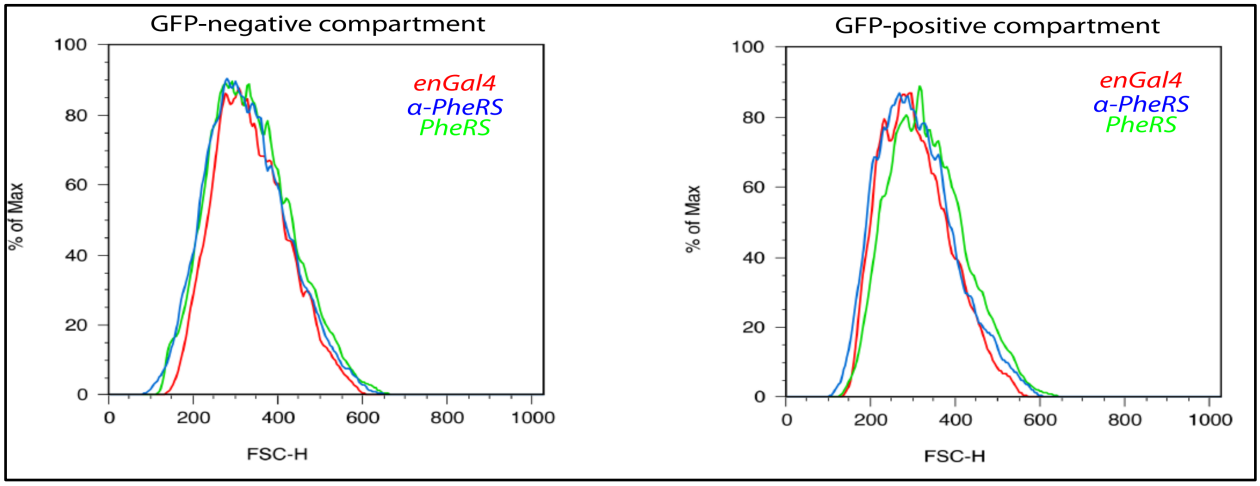

B

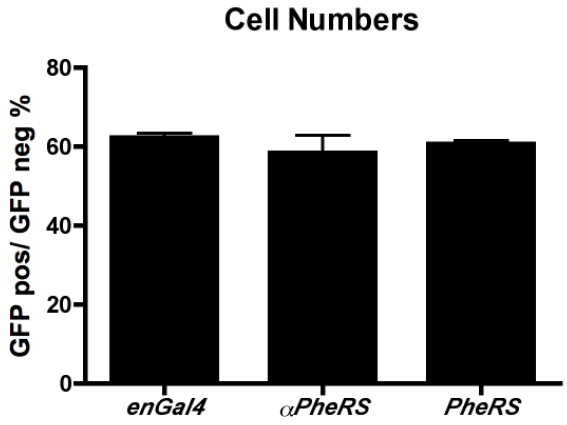

Figure S2: PheRS overexpression in wing discs increases cell size, but not cell numbers
(A) Cell size was determined by measuring the Forward Scatter (FSC) in the FACS analysis. Larvae were synchronized by using 2-hours egg lays. Late 3rd instar larvae were dissected and wing discs were dissociated. GFP was used to mark cell populations that express transgenes. The cells of the GFP-negative compartment showed similar cell size in the different lines (left panel). In the GFP positive compartment, where the transgenes were overexpressed, PheRS overexpression gave rise to bigger cells (right panel). The graph represents the results of three independent experiments. (B) Cell numbers are not significantly altered by PheRS overexpression. The experimental set up was the same as in (A). Posterior cell numbers (P; GFP positive) were determined relative to the anterior (A; GFP negative) cell numbers (n=3).

Supplementary Figure S3

Amino acid deprivation downregulates phosphorylation of dS6K in Kc cells, and subsequent stimulation with amino acids can restore this phosphorylation (Kim et al., 2008). The Rag complex is part of a nutrient sensor pathway, and its knockdown prevents the TORC1 complex from sensing the availability of amino acids (Kim et al., 2008; Sancak et al., 2008). In contrast, when *β-PheRS* was knocked down, amino acids were still able to induce phosphorylation of dS6K to similar levels as in the control. In this case, it did not matter whether all amino acids were added back (A) or only L-Phe (B). These results therefore suggest that PheRS does not serve as an amino acid sensor upstream of the TORC1 complex, although we cannot rule out that the knockdown was not sufficient to induce this effect.

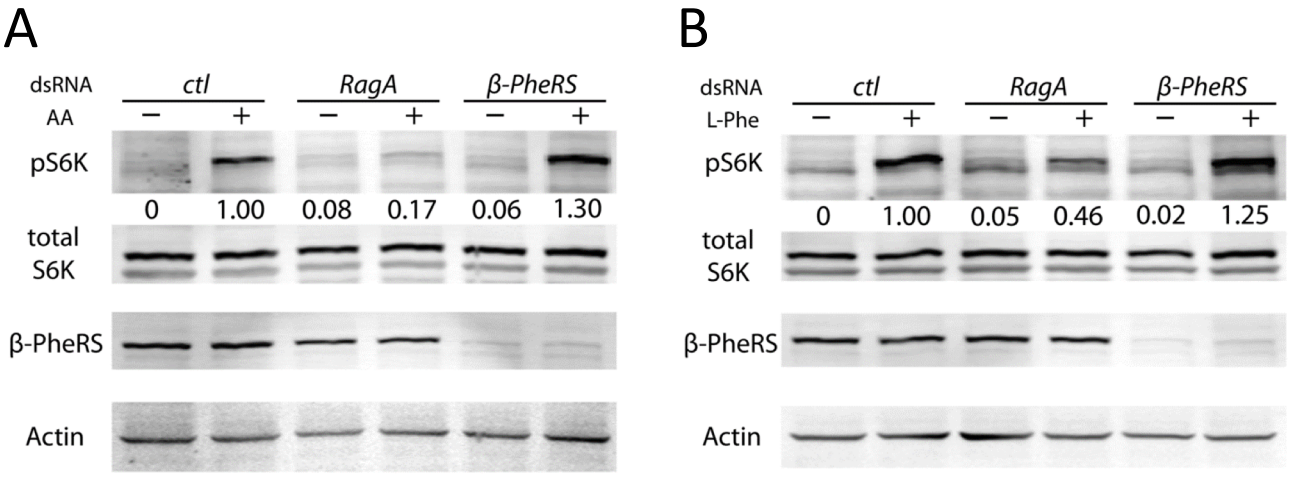

Figure S3: PheRS does not seem to serve as an amino acid sensor upstream of the TORC1 complex. (A) *β-PheRS* knockdown cannot block the TORC1 complex from sensing the availability of amino acids. Phospho-S6K was used as a readout of TORC1 signaling. Starvation (–) was performed by depriving cells from amino acids for 30 mins, and stimulation (+) was performed by adding back amino acids for 30 mins after starvation. Control is a mock RNAi *RagA* RNAi is known to block the sensing of amino acids. The level of phospho-S6K was quantified relative to the Actin level in the same extract. (B) *β-PheRS* knockdown cannot block the TORC1 complex from sensing the availability of L-Phe. The same experiment as in (A) was performed, but using L-Phe and L-Glu for stimulation. L-Glu was reported to be necessary for amino acid transport (Nicklin et al., 2009). Levels of phospho-S6K were quantified relative to the Actin levels in the same extract.

Reference

Kim, E., Goraksha-Hicks, P., Li, L., Neufeld, T.P., Guan, K.L., 2008. Regulation of TORC1 by Rag GTPases in nutrient response. Nature cell biology 10, 935-945.

Nicklin, P., Bergman, P., Zhang, B., Triantafellow, E., Wang, H., Nyfeler, B., Yang, H., Hild, M., Kung, C., Wilson, C., Myer, V.E., MacKeigan, J.P., Porter, J.A., Wang, Y.K., Cantley, L.C., Finan, P.M., Murphy, L.O., 2009. Bidirectional transport of amino acids regulates mTOR and autophagy. Cell 136, 521-534.

Sancak, Y., Peterson, T.R., Shaul, Y.D., Lindquist, R.A., Thoreen, C.C., Bar-Peled, L., Sabatini, D.M., 2008. The Rag GTPases bind raptor and mediate amino acid signaling to mTORC1. Science 320, 1496-1501.

Supplementary Figure S4

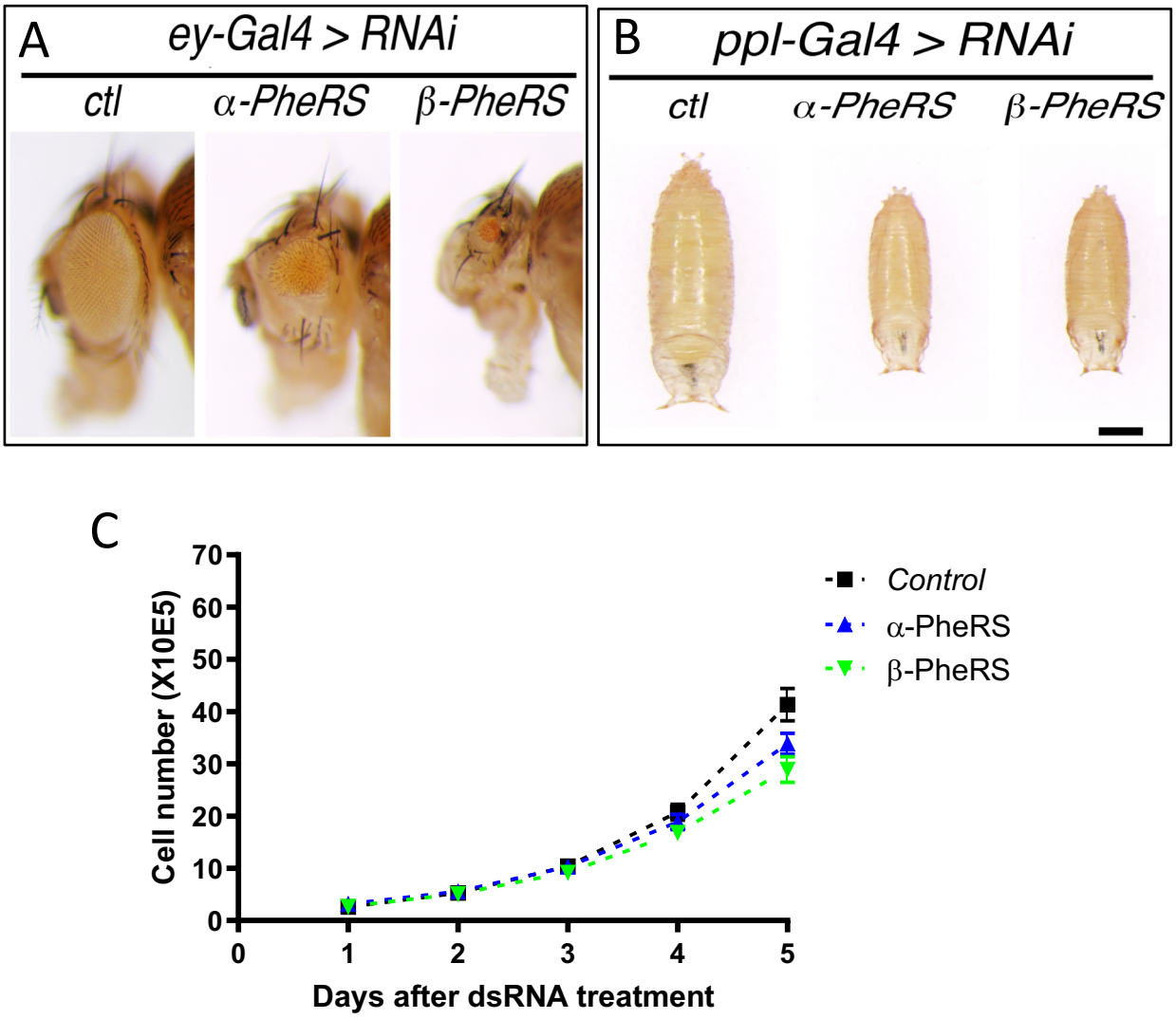

Figure S4: PheRS knockdown reduces cell proliferation and tissue size.
(A,B) RNAi knock down of *PheRS* subunits in the fly eyes (A) and fat bodies (B). *ey-Gal4* and *ppl-Gal4* were used to drive RNAi expression, respectively. The controls were GFP RNAi. RNAi knock down of either subunit reduced the eye size (A) and the size of the entire pupae, respectively. (C) Proliferation of Kc cells upon knockdown of the subunits. The control is mock RNAi. RNAi knockdown was carried out by directly adding dsRNA to the medium, and cells were harvested at days 1, 2, 3, 4, and 5 after dsRNA treatment. Knockdown of either subunit reduces cell proliferation and downregulates levels of both subunits (Lu et al., 2014).

Reference

Lu, J., Bergert, M., Walther, A., Suter, B., 2014. Double-sieving-defective aminoacyl-tRNA synthetase causes protein mistranslation and affects cellular physiology and development. Nature communications 5, 5650.

Supplementary Figure S5

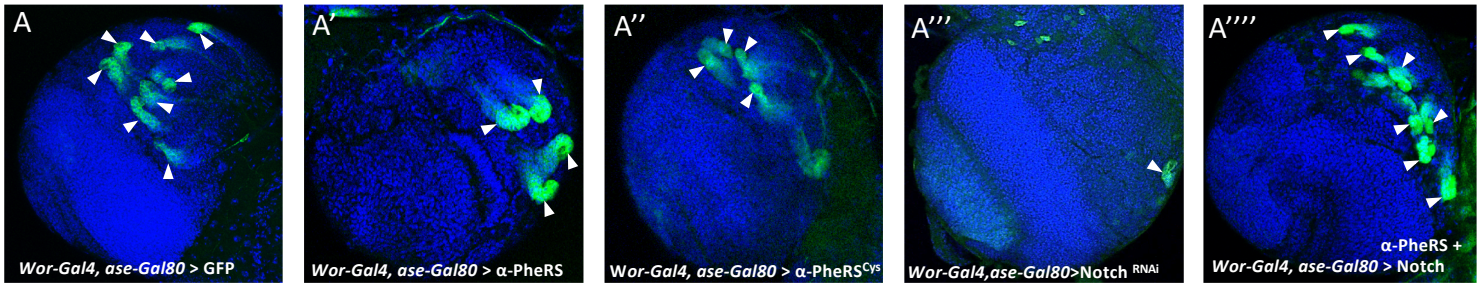

Figure S5: Overexpression of *α-PheRS* or *α-PheRS^{Cys}* in type II NBs reduced the number of type II NBs per central brain. *wor-Gal4,ase-Gal80,UAS-GFP* was used to overexpress proteins in marked (GFP signal) type II NBs. Type II NBs are pointed out with white arrowheads.